
# Clustering of Regional-Scale Extreme Precipitation Events in Southern Switzerland

YANNICK BARTON AND PARASKEVI GIANNAKAKI

*Institute of Geography and Oeschger Center for Climate Change Research, University of Bern, Bern, Switzerland*

HARALD VON WALDOW

*Centre for Climate Systems Modeling, ETH Zürich, Zurich, Switzerland*

CLÉMENT CHEVALIER

*Institute of Mathematics, University of Zurich, Zurich, Switzerland*

STEPHAN PFAHL

*Institute for Atmospheric and Climate Science, ETH Zürich, Zurich, Switzerland*

OLIVIA MARTIUS

*Institute of Geography, Mobiliar Lab for Natural Risks and Oeschger Centre for Climate Change Research, University of Bern, Bern, Switzerland*

(Manuscript received 29 May 2015, in final form 21 September 2015)

ABSTRACT

Temporal clustering of extreme precipitation events on subseasonal time scales is of crucial importance for the formation of large-scale flood events. Here, the temporal clustering of regional-scale extreme precipitation events in southern Switzerland is studied. These precipitation events are relevant for the flooding of lakes in southern Switzerland and northern Italy. This research determines whether temporal clustering is present and then identifies the dynamics that are responsible for the clustering.

An observation-based gridded precipitation dataset of Swiss daily rainfall sums and ECMWF reanalysis datasets are used. Also used is a modified version of Ripley's $K$ function, which determines the average number of extreme events in a time period, to characterize temporal clustering on subseasonal time scales and to determine the statistical significance of the clustering. Significant clustering of regional-scale precipitation extremes is found on subseasonal time scales during the fall season.

Four high-impact clustering episodes are then selected and the dynamics responsible for the clustering are examined. During the four clustering episodes, all heavy precipitation events were associated with an upper-level breaking Rossby wave over western Europe and in most cases strong diabatic processes upstream over the Atlantic played a role in the amplification of these breaking waves. Atmospheric blocking downstream over eastern Europe supported this wave breaking during two of the clustering episodes. During one of the clustering periods, several extratropical transitions of tropical cyclones in the Atlantic contributed to the formation of high-amplitude ridges over the Atlantic basin and downstream wave breaking. During another event, blocking over Alaska assisted the phase locking of the Rossby waves downstream over the Atlantic.

## 1. Introduction

Regional-scale extreme precipitation events in the mountainous terrain of the Alpine region can have severe impacts on human populations and the environment (Frei

*Corresponding author address*: Yannick Barton, Institute of Geography and Oeschger Centre for Climate Change Research, University of Bern, Hallerstr. 12, 3012 Bern, Switzerland.
E-mail: yw.barton@gmail.com

DOI: 10.1175/MWR-D-15-0205.1

et al. 2000). They can trigger floods, which are the main natural hazard in terms of financial damage in Switzerland (Hilker et al. 2009). The potential damage of these regional-scale extreme precipitation events can be substantial because they can affect the entire watershed of a river or a lake. For example, in September 1993 a 3-day extreme precipitation event in the southern Swiss mountains caused the Saltina River to leave its riverbed, resulting in approximately 750 million Swiss francs in damages and killing two people in the town of Brig (Badoux and Rickenmann 2008). A succession of such regional-scale extreme precipitation events occurring over a short period of time can be associated with several implications, as discussed below.

First, the succession of heavy precipitation events can lead to flood events in rivers and catchments with a high retention capacity. In fall 1993 in Switzerland, a series of extreme precipitation events followed the Brig event in close succession until mid-October. Record 10- to 30-day precipitation sums occurred during this time period (BAFU 1994), resulting in a centennial maximum water level of Lago Maggiore in southern Switzerland and causing the lake to repeatedly overflow. Recent other examples in which several extreme precipitation events in short temporal succession resulted in high-impact flood events are the severe floods in central Europe in summer 2013 (Grams et al. 2014), the floods in Pakistan in summer 2010 (Galarneau et al. 2012; Martius et al. 2013), and the floods in England in the winter 2014 (Huntingford et al. 2014).

Second, the short recovery time between events can overburden rescue teams and prevent proper clean-up of damages and efficient repairing of damaged protective structures. Moreover, the temporal clustering and hence temporal dependence of precipitation and other extremes is of interest for insurance companies as their loss models are typically based on independence assumptions. In this study, we focus on the temporal clustering of extreme regional-scale precipitation events in southern Switzerland that are, among other high impacts, relevant for the flooding of Lago Maggiore.

A number of studies have analyzed the statistical properties of the temporal clustering of extreme events, namely European winter storms (e.g., Mailier et al. 2006; Vitolo et al. 2009; Pinto et al. 2013) and extreme precipitation in the North American Midwest (Villarini et al. 2011). In those studies, clustering in time was assessed using a one-dimensional homogeneous Poisson process model (i.e., a Poisson process with a constant intensity of events). The temporal clustering of regional-scale heavy precipitation in southern Switzerland has so far not been investigated. To study the processes behind temporal clustering, it is necessary to first assess if regional-scale heavy precipitation events in southern Switzerland exhibit statistically significant clustering on different subseasonal time scales, which constitutes the first aim of this paper.

Once the presence of clustering in time is statistically established, the synoptic-scale dynamics responsible for the clustering will be investigated. For the clustering of extreme European winter storms, the meridional extent and the strength of the North Atlantic extratropical jet are of central importance (Pinto et al. 2014), as well as the phase of the North Atlantic Oscillation (NAO) (e.g., Mailier et al. 2006; Vitolo et al. 2009). The NAO also plays an important role for the temporal clustering of heavy precipitation in the Midwest (Villarini et al. 2011).

The synoptic-scale triggers of individual regional-scale extreme precipitation events in the southern Swiss Alps are well known. These events mainly occur in a conditionally unstable environment, when a moist air mass is advected in a southerly flow toward the Alpine ridge and then orographically forced to ascend (e.g., Massacand et al. 1998; Martius et al. 2006b). The low-level southerly flow, typically transporting moisture from the Atlantic Ocean and the Mediterranean Sea (Winschall et al. 2014), can be related to the presence of a positive upper-tropospheric potential vorticity (PV) anomaly over western Europe (Doswell et al. 1998; Massacand et al. 1998; Martius et al. 2006b). These anomalies form through Rossby wave breaking (RWB) over the eastern Atlantic and western Europe and take the shape of a meridionally elongated PV trough (streamer), a cutoff, or, in a few cases, a broad trough (Martius et al. 2006b) (see also Fig. 1).

Massacand et al. (2001) showed that a strong ridge located upstream over the central Atlantic can support the wave breaking over western Europe. This ridge can in turn be amplified by strong upstream cyclogenesis with strong latent heat release in the warm conveyor belt (WCB) and attendant diabatic upper-level PV reduction (Massacand et al. 2001; Madonna et al. 2014b) or by transitioning tropical cyclones (Grams et al. 2011; Archambault et al. 2013). A tropical cyclone undergoing extratropical transition can lead to an amplification of an extratropical ridge downstream through the advection of tropospheric low PV by the divergent outflow of the tropical cyclone [see Riemer et al. (2008) and Archambault et al. (2013) for more details] and through the diabatic reduction of PV in the outflow region of a tropical cyclone.

The upstream ridge over the central Atlantic is sometimes part of a Rossby wave train emerging from farther upstream. Indeed, breaking Rossby waves associated with extreme precipitation in southern Switzerland in fall and winter are typically preceded by a precursor Rossby wave signal that formed up to a week prior in the central and eastern Pacific (Martius et al. 2008).

In summary, individual regional-scale extreme precipitation events over southern Switzerland have been

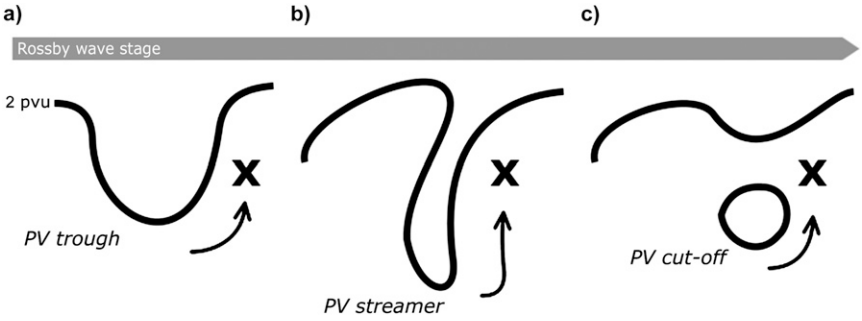


FIG. 1. Schematic showing the (a) linear and (b),(c) breaking stages in the life cycle of a Rossby wave. During these stages, the dynamical tropopause (2-PVU line) usually takes the shape of a trough [in (a)], a streamer [in (b)], or a cutoff. During extreme precipitation events in southern Switzerland, such upper-level flow structures are typically located to the west of the Alps (the Alps are marked with an ×). The associated low-level flow direction is indicated by the arrows.

related to large-scale atmospheric precursors upstream of the events [see also Martius et al. (2008)] and are well predictable (Grazzini 2007). It is, however, an open question if the same dynamics are relevant during time periods when temporal clustering occurs (i.e., when several regional-scale extreme precipitation events occur in close succession), and it is an open question why the conditions that lead to individual extreme precipitation events form recurrently over a relatively short time period. Here, we address these open questions; the second and third aims of this paper are hence to describe the local upper-level flow and the upstream flow conditions during clustering periods of extreme regional-scale precipitation events in southern Switzerland, and to understand why these large-scale flow conditions formed recurrently within one season.

## 2. Data and methods

### *a. Meteorological and hydrological datasets*

We used 1 km × 1 km gridded daily precipitation data for Switzerland. This gridded dataset is based on over 420 rain gauge measurements and covers the time period from 1961 to the present (Frei and Schär 1998; MeteoSwiss 2013). From the gridded dataset, we calculated an area-averaged daily precipitation time series for southern Switzerland using the ''south of the Alps'' region defined by Fischer et al. (2012) (see also Fig. 2 herein), which is similar to the area used in Martius et al. (2006b). This area corresponds approximately to the watershed that drains into Lago Maggiore; it does, however, not include the parts of the watershed that are located in Italy. The spatial averaging deemphasizes strongly localized extreme precipitation events and puts the focus on the watershed-wide precipitation extremes that are relevant for flooding of Lago Maggiore.

To study the large-scale atmospheric flow, we used ECMWF's ERA-40 (Uppala et al. 2005) and ERA-Interim (Dee et al. 2011) datasets. Both reanalysis datasets are interpolated to a 1° × 1° spatial grid. They have a temporal resolution of 6 h and 60 vertical model levels ranging from the surface to 0.1 hPa. To calculate climatological reference fields, we used ERA-40 data from 1961 to 1990 and ERA-Interim data from 1981 to 2010. Percentiles of the vertically integrated moisture flux were calculated to investigate the moisture transport associated with extreme precipitation events and to put it into a climatological perspective. For this, we used 6-hourly data within one month from 1981 to 2010 for every grid point. The same procedure is applied for the precipitable water. Hovmöller diagrams of the meridional wind along the dynamical tropopause were calculated on the 325-K isentropic surface following the method of Martius et al. (2006a).

To identify atmospheric blocking events, a two-dimensional blocking index was derived from the ERA-40 and ERA-Interim datasets. The blocking identification is based on negative PV anomalies in the middle to upper troposphere and takes into account the three-dimensional structure of the phenomenon (Schwierz et al. 2004). This index requires a minimum blocking lifetime of five days.

Warm conveyor belt outflow is detected following the procedure outlined in detail in Madonna et al. (2014a). In brief, WCB air parcels (i.e., air parcels undergoing an ascent of 600 hPa and more in 48 h) in the vicinity of a cyclone are identified (Madonna et al. 2014b). At every instance in time only the WCB air parcels above the 310-K isentrope and in a time window of 36–72 h after starting their ascent are selected. Coherent regions with WCB air parcels are marked as WCB outflow objects. The WCB objects are collocated with and point to areas of diabatically reduced PV as the WCB air parcels have

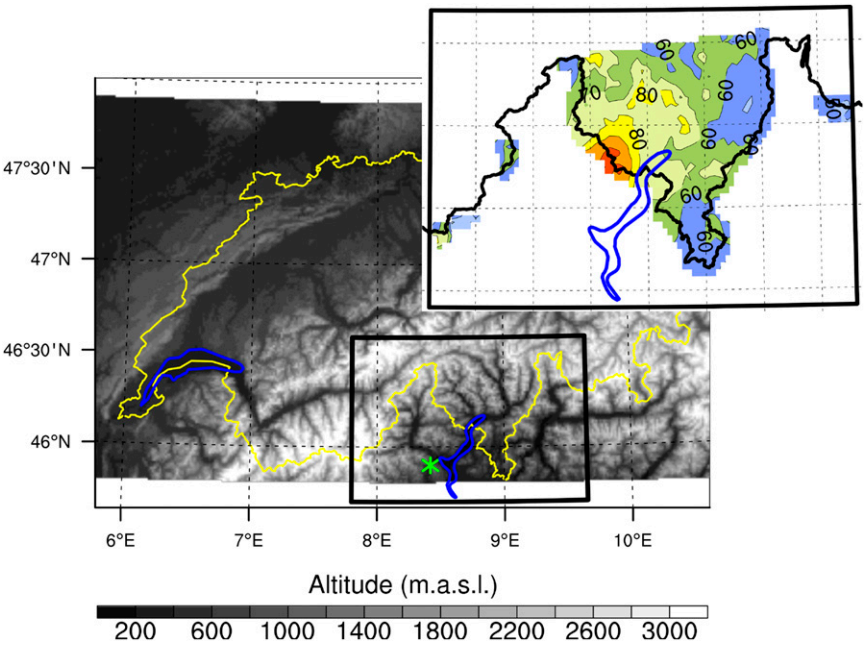


FIG. 2. The gray shading shows the elevation of the Swiss topography. The color shading illustrates the 99th precipitation percentile of the mean daily precipitation accumulation (mm) from 1961 to 2010 for southern Switzerland and shows the study area. Blue contours indicate major Swiss lakes. The Lago Maggiore is indicated by the green star.

moved through areas of strong diabatic heating before they reached the upper troposphere.

For information on tropical cyclone best track data, we used the IBTrACS dataset (Knapp et al. 2010). Only the quality-checked data from WMO agencies were used. The activity of the Madden–Julian oscillation (MJO) was assessed based on the daily MJO index developed by Wheeler and Hendon (2004) and provided by the Australian Bureau of Meteorology (BOM) through their website (http://www.bom.gov.au/climate/mjo/). To study the water level of the Lago Maggiore, the Locarno station daily mean water level data were used. The data from 1961 to 2012 were provided by the Swiss Federal Office for the Environment. Outgoing longwave radiation (OLR) information stems from the Liebmann and Smith (1996) dataset. Finally, globally merged (70°N–70°S) gridded (8-km grid spacing) infrared brightness temperature data from the International Satellite Cloud Climatology Project (ISCCP) were used (Knapp 2008).

### b. *Statistical procedures*

Daily precipitation sums may exhibit temporal dependence, even at high quantiles. In southern Switzerland regional-scale precipitation extremes are triggered by long-lived synoptic systems (Hoinka et al. 2006; Pfahl and Wernli 2012). This leads to temporal clusters of extreme precipitation days on the time scale of the synoptic systems. Here, we are interested in the time-varying rate of precipitation extremes on longer, subseasonal time scales. We therefore aim to first filter the daily precipitation time series in order to remove this interday dependency, hereafter called "high-frequency clustering."

To that end, we employ a method from the standard repertoire of extreme value statistics, the "runs declustering," which is commonly applied in the analysis of precipitation extremes with the peak-over-threshold (POT) approach (Coles 2001). Given a run length $r$ and a threshold $u$, exceedances of $u$ that are separated by less than $r$ values below $u$ are assumed to belong to one cluster. All exceedances of that cluster are then replaced by its maximum exceedance to yield a series of independent occurrences of extreme precipitation events.

To determine the run length $r$, we use the method of Ferro and Segers (2003), who estimate the extremal index, from which the run length can be calculated, based on a result regarding the asymptotic distribution of the times between threshold exceedances. The threshold $u$ has to be set a priori. This choice is inherently challenging in the context of POT analyses, as it influences the estimate of $r$, and hence the subsequent estimate of return levels (Süveges and Davison 2010). However, since such an analysis is not our goal, we follow a practical approach and apply the runs declustering for three different thresholds, the 95th, 98th, and 99th percentiles of the daily precipitation accumulation of all days.

These thresholds are consistent with the threshold selection plots recommended by Coles (2001) and have been applied before to Swiss precipitation time series (Fukutome et al. 2015). We found a maximum declustering run length $r$ of about two days for all thresholds and all seasons, which is in good agreement with previous analyses: Fukutome et al. (2015) found $r$ to lie between 20 and 40 h (winter) and 10 and 20 h (summer) in the southern Alps. Hoinka et al. (2006) report that strong precipitation events at the south side of the Alps have a lifetime of one to two days in fall. With our value of two days, we are at the more conservative end of the range.

To study clustering of extreme precipitation events on longer, subseasonal time scales, we apply Ripley's $K$ function (Ripley 1981). Ripley's $K$ is a cumulative function typically used to examine the clustering behavior of spatial point patterns at different spatial scales (Haase 1995), but it can also be applied in one dimension, as we do here, to study temporal clustering of events on the time axis (Dixon 2002). Ripley's $K$ can be regarded as the average number $E(t)$ of extra events (i.e., extreme precipitation events) within time $t$ around a randomly chosen event and is defined mathematically as

$$K(t) = \lambda^{-1} E(t),$$

where $\lambda$ is the density of events (Dixon 2002). For simplicity, we drop $\lambda^{-1}$, since it does not affect the results as long as the same estimator is applied to the empirical and simulated data. We estimate $K$ as

$$\hat{K}(t) = \frac{1}{n} \sum_{i=1}^{n} \sum_{j \neq i} I_{|ti-tj| \leq t},$$

where $n$ is the total number of events, $t_i$ is the time of an extreme event, $t_j$ are the times of occurrence of all other extreme events of the same year as $t_i$ and $I$ is the indicator function:

$$I_{|ti-tj| \leq t} = \begin{cases} 1 & \text{if} \quad |ti - tj| \leq t \\ 0 & \text{if} \quad |ti - tj| > t \end{cases}.$$

We measure the significance of the clustering of extreme precipitation event occurrences by comparing $\hat{K}(t)$ with Ripley's $K$ calculated from a Monte Carlo simulation of a homogeneous Poisson process, $K^{\mathrm{MC}}(t)$. The comparison with a homogeneous Poisson process (i.e., when events occur independently from each other at a constant rate) has been used before to assess clustering of extreme precipitation (Villarini et al. 2011) and severe storms (Mailier et al. 2006; Vitolo et al. 2009). Temporal clustering is assessed at different time scales $t$, as we are interested in identifying which time scales reveal significant clustering. The calculations are performed separately for the four seasons—winter [December–February (DJF)], spring [March–May (MAM)], summer [June–August (JJA)], and fall [September–November (SON)]—in order to avoid the effects of the seasonal cycle present in the precipitation event counts into the estimation of $\hat{K}(t)$.

The intensity of the homogeneous Poisson process used for the MC simulation is estimated from the observed data. For any given $t$, if the estimated $\hat{K}(t)$ from the observed data is greater than the 95th percentile of the simulated $K^{\mathrm{MC}}(t)$, the data are significantly clustered. If $\hat{K}(t)$ is lower than the 5th percentile of $K^{\mathrm{MC}}(t)$, the data are significantly regularly spaced. If $\hat{K}(t)$ is within the confidence interval of $K^{\mathrm{MC}}(t)$ for a given $t$, the data are consistent with a homogeneous Poisson process. The calculations are performed with varying time scales $t$, ranging from one day to half of the length of a season (~45 days). To avoid artificial clustering across different years, the calculations are performed for each year separately; only event occurrences of a same year are considered. The same procedure was used in the Monte Carlo simulations.

## 3. Results

The results section is separated into two parts. The first part contains the results of the statistical analysis; the second part discusses the atmospheric flow during four selected low-frequency clustering periods.

### *a. Poisson point analysis*

As stated in the introduction, the first aim of this paper is to determine whether low-frequency clustering is present in the precipitation time series from southern Switzerland. During winter, spring, and summer the declustered extreme precipitation events (i.e., after removal of "high-frequency" clustering) are not statistically significantly clustering in time (not shown); we focus thereafter on the fall season.

For the nondeclustered time series, we find statistically significant clustering for all time scales and all percentile thresholds (Figs. 3a–d). In the declustered time series, significant clustering is found for the 99th percentile threshold and above on time scales from 10 days up to 30 days (Figs. 3g,h). No statistically significant clustering is found for the 95th and 98th percentile thresholds (Figs. 3e,f). Note that the relatively low number of events for thresholds above the 99th percentile level is included in the uncertainty estimation and reflected in a widening of the confidence band.

Note that because of the cumulative properties of the $K$ function, clustering at shorter time scales affects

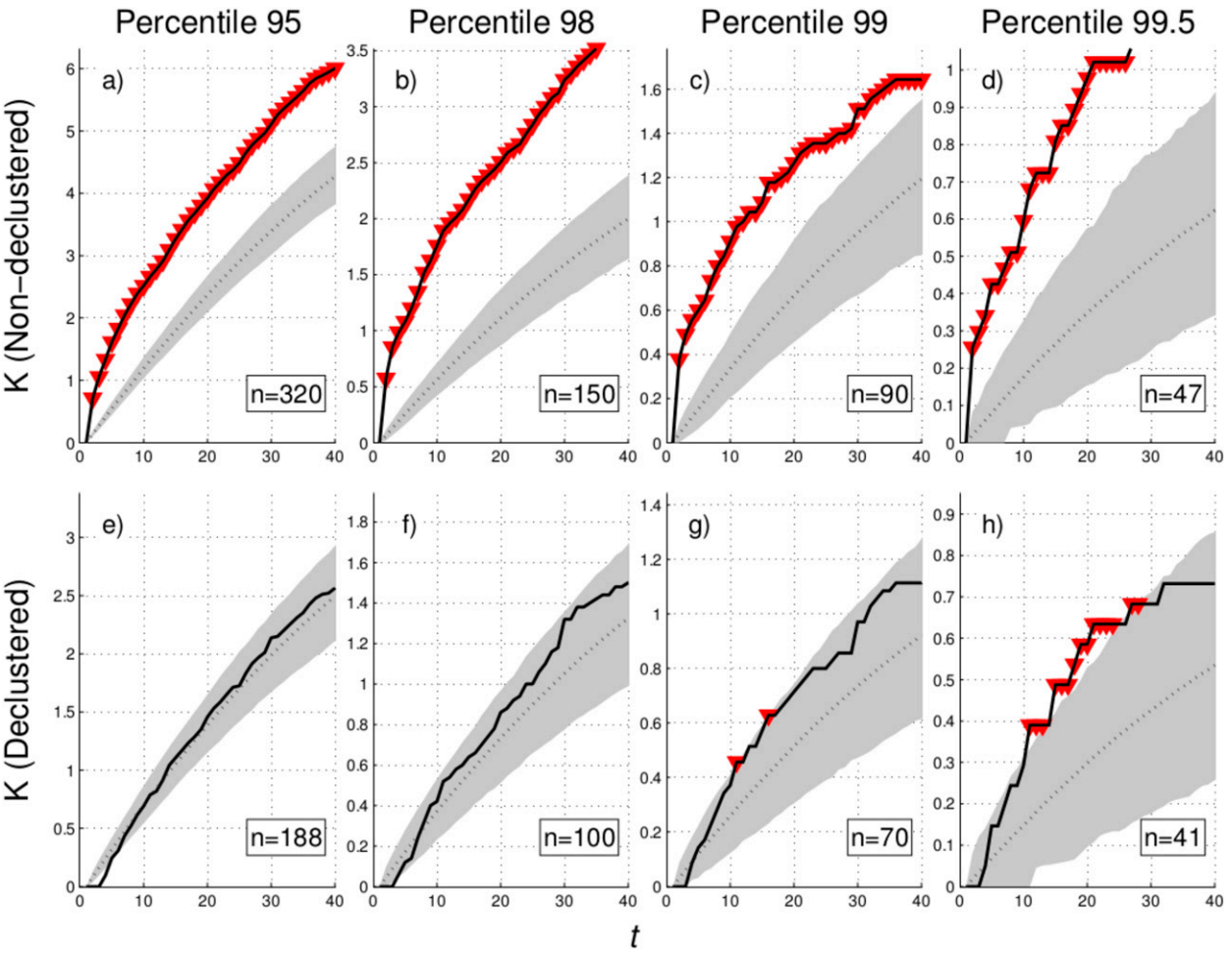


FIG. 3. Ripley's $K$ values for the fall season (SON) with MC confidence intervals (shaded area, 5th–95th percentile) for the (a),(e) 95th; (b),(f) 98th; (c),(g) 99th; and (d),(h) 99.5th precipitation percentile and for time scales $t$ ranging from 1 to 40 days. The solid line illustrates the Ripley's $K$ function based on the observed data. The dotted line is the mean simulated $K$ function. Red triangles indicate significant values at the 10% confidence level. (top) Original time series; (bottom) time series with the high-frequency clustering removed. The total number of considered events $n$ is indicated at the bottom right of each plot.

clustering at longer time scales; the clustering at a shorter time scale can lift $K$ at longer time scales outside the MC confidence band (this is taken into account in the width of the confidence interval that increases with an increasing time scale). Therefore, the relatively steep slope of the observed $K$ function for time scales up to 10 days in the declustered time series suggests that the significant clustering at subsequent time scales is mainly the manifestation of clustering at the 10-day time scale. The bulk of the clustering in the nondeclustered time series is to be attributed to high-frequency clustering, which reflects the comparatively large amount of consecutive extreme days. The declustering proves its effectiveness and is demonstrated for $t \leq 3$ where $K = 0$ (Fig. 3, bottom row).

In summary, statistically significant clustering of regional-scale extreme precipitation events in southern Switzerland is found on subseasonal time scales even when using a very conservative approach in which the effect of the high-frequency clustering (i.e., the occurrence of extremes on consecutive days due to the lifetime of weather systems) is excluded from the time series.

### b. *Selection of clustering periods*

In a next step, we identified the submonthly time periods containing the largest number of extreme precipitation events and studied these episodes in more detail. To this end, we counted the number of very heavy (>98th percentile) and extreme (>99th percentile) precipitation events in a moving window of three

TABLE 1. This table shows the sorted counts of 99th (99p) and 98th (98p) percentile precipitation events as well as sorted amounts for 14-, 21- and 28-day windows. The dates indicate the beginning of a clustering period. For example, 24 Sep 1993 was the first day of a 21-day period with four occurrences of events that exceeded the 99th percentile. The selected clustering periods are in boldface.

| | 99p (60 mm) | | | 98p (46 mm) | | |
|---|---|---|---|---|---|---|
| Window | Date | No. | Amount (mm) | Date | No. | Amount (mm) |
| 14 | 2 Oct 1993 | 3 | 475 | **15 Nov 2002** | 3 | 601 |
| | | | | 2 Oct 1993 | 3 | 475 |
| | | | | 21 Jun 1997 | 3 | 375 |
| | | | | 20 Sep 1999 | 3 | 340 |
| | | | | 23 May 2002 | 3 | 250 |
| 21 | **24 Sep 1993** | 4 | 721 | 24 Sep 1993 | 4 | 721 |
| | **22 Aug 1965** | 3 | 536 | 15 Nov 2002 | 3 | 613 |
| | 30 Sep 2000 | 3 | 496 | 13 Sep 1993 | 3 | 574 |
| | | | | 28 Sep 1976 | 3 | 515 |
| | | | | 22 Aug 1965 | 3 | 496 |
| 28 | 24 Sep 1993 | 4 | 782 | 13 Sep 1993 | 4 | 812 |
| | **20 Sep 2000** | 4 | 602 | 31 Oct 2000 | 4 | 782 |
| | | | | 26 Apr 1983 | 3 | 638 |
| | | | | 15 Nov 2002 | 3 | 618 |
| | | | | 28 Sep 1976 | 3 | 549 |

subjectively chosen but hydrologically relevant lengths (14, 21, and 28 days). The moving window was shifted from 1 January 1961 to 31 December 2010 with an increment of one day. Table 1 shows the top five clustering periods of very heavy and extreme precipitation events for 14-, 21-, and 28-day moving windows. The dates correspond to the starting time of a clustering period. Overlapping time periods are aggregated and the episode with the largest number of events is considered.

For a window length of 21 days, one episode contains four extreme precipitation events above the 99th precipitation percentile (24 September 1993); two additional episodes contain three events above the 99th percentile (30 September 2000 and 22 August 1965). For this window length, all remaining clustering periods contain less than three extreme precipitation events. Note that almost all episodes containing more than two extreme events occurred in fall (one in August). If the 98th percentile events are included, a few clustering periods can be observed in late spring, as well as in early and late summer; none of the identified clustering periods occurred during winter.

Out of these clustering periods, we selected the top four periods in terms of event counts and societal impacts to study the dynamics related to the low-frequency clustering. This selection relies partially on a subjective decision; however, we focus on the episodes with the severest impacts while still having a sample that represents the wide range of processes involved with and responsible for the clustering. We select the three time periods with three and more exceedances above the 99th percentile (21 August–11 September 1965, 22 September–15 October 1993, and 19 September–16 October 2000) and the episode with the largest count of events above the 98th precipitation percentile in a window length of 14 days with the greatest accumulated precipitation over that period of time (13–27 November 2002). Note that the beginnings of the selected time periods do not correspond to the event maxima, but rather to the starting time of the first event. It should also be noted that the summer/fall 1965 event is part of the fall season time series evaluated in the Poisson analysis as we add days at the beginning and end of each season to account for edge effects (see also section 2b).

### c. *Precipitation characteristics of the selected clustering periods*

Figure 4 shows the daily precipitation accumulation during the four selected periods. The time period of September–October 1993 exhibited an exceptionally high count of extreme precipitation events (>99th percentile): four extreme precipitation events occurred over a 21-day time period. During September–October 2000, four extreme events occurred over a 28-day time period. In November 2002, a 14-day time period of continuous precipitation included two extreme and one very heavy (>98th) precipitation events and the largest 14-day precipitation accumulation (601 mm) between 1961 and 2010. By comparison, the monthly climatological precipitation of November in southern Switzerland is 166 mm. Additionally, the fourth largest daily precipitation sum of the entire precipitation time series was recorded on 15 November 2002. In August and September 1965 three extreme precipitation events occurred within a 21-day period. It should be noted that

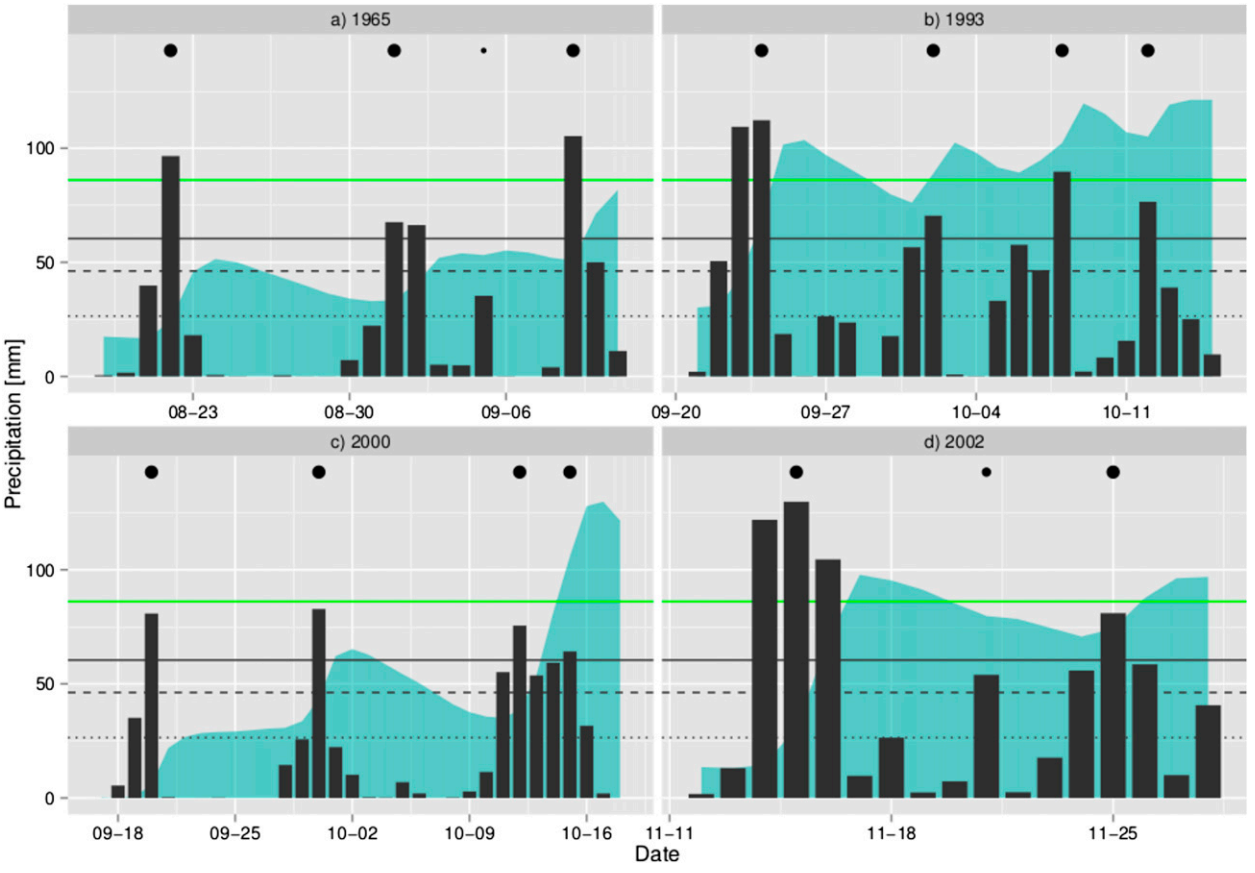


FIG. 4. Daily precipitation sums (black bars) for four selected clustering periods (1965, 1993, 2000, and 2002) are shown with 95th (dotted line), 98th (dashed line), and 99th (solid line) precipitation thresholds. The large, medium, and small circles show the extreme (99p), very heavy (98p), and heavy (95p) precipitation event maxima after declustering, respectively. The blue shaded area indicates the mean daily water level of Lago Maggiore measured at the Locarno station. The green line indicates the 195.75 m MSL threshold of the Lago Maggiore water level.

most of the identified extreme precipitation events affected not only southern Switzerland, but also surrounding regions in Switzerland and Italy.

The majority of southern Switzerland's rivers drain into Lago Maggiore; it is therefore interesting to look at the impact of the clustering of heavy precipitation events on the lake level (see Fig. 4, blue shading). The extreme precipitation events were typically followed by a relatively rapid rise of the water level one or two days after the event. During each clustering episode (with the exception of 1965), the lake level reached the critical flooding level of 197.5 m MSL (green line in Fig. 4), above which significant damage is expected. The recovery time of the lake's water level is relatively slow; during all clustering episodes, the lake level did not recede back to the level prior to the clustering episode in the time between two successive extreme precipitation events. Each precipitation event therefore resulted in a further increase of the lake level. This effect was especially pronounced during the 1993 clustering event. The clustering of extreme precipitation events on a 20- to 30-day time scale hence systematically increases the risk of flooding. We will discuss the synoptic dynamics that resulted in the clustering of heavy precipitation events during these four periods in more detail in the next sections.

### *d. Local precipitation precursors*

To understand the local triggers of the regional-scale extreme precipitation events in southern Switzerland, we look at the upper-level flow over western Europe. Figure 5 shows the upper-level PV fields on extreme precipitation event days during all four clustering periods. We first look at the most extreme episode in fall 1993. On 22 September 1993, an elongated streamer of high-PV air extended over the Iberian Peninsula to northern Africa [see also Massacand et al. (1998)]. This streamer developed into a cutoff centered over the western Mediterranean Sea on 23 September, and high moisture fluxes (>99%) toward the Alps were present

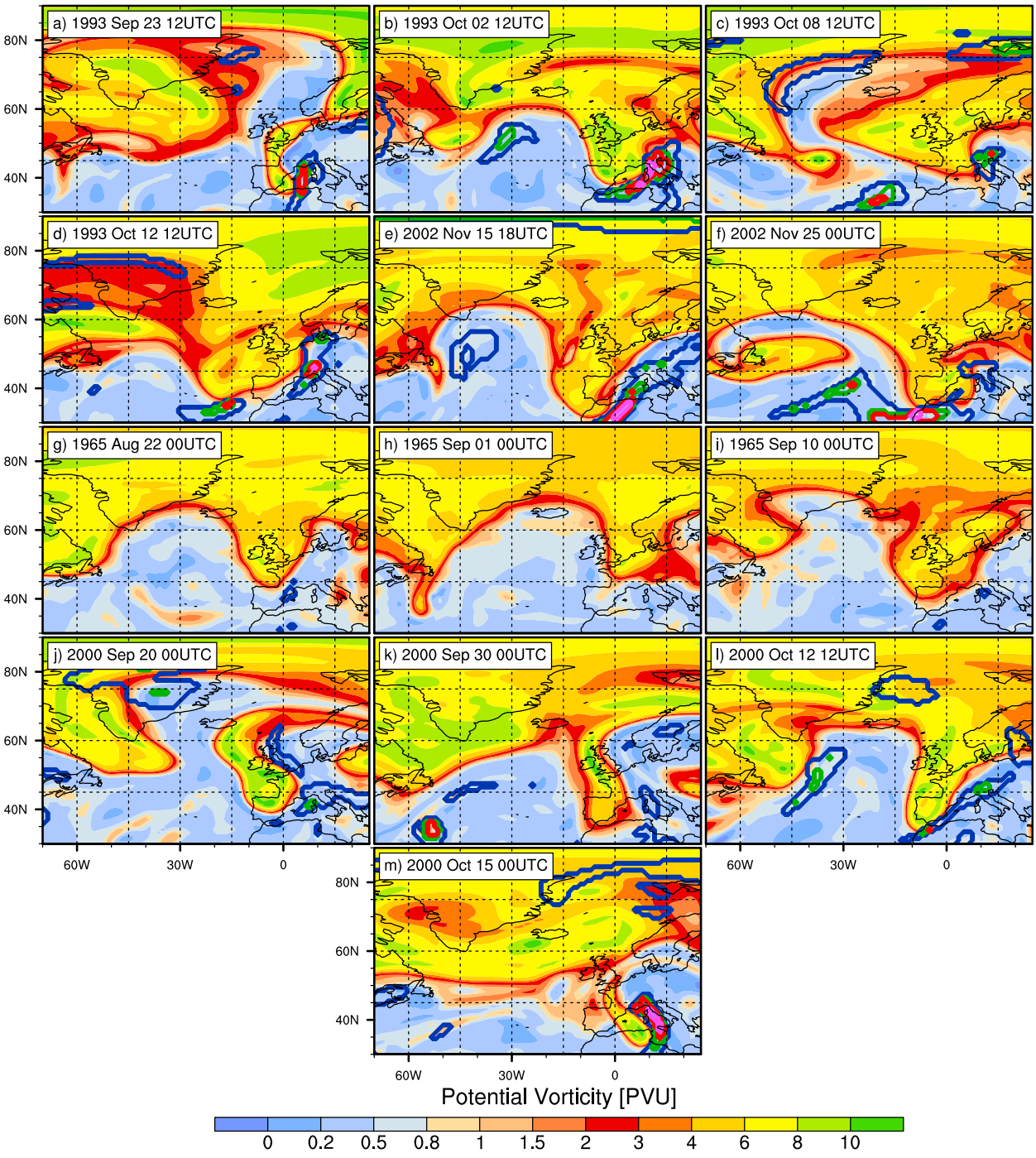


FIG. 5. PV field on the 330-K isentrope in August, on the 325-K isentrope in September and October, and on the 320-K isentrope in November for each extreme precipitation event of the four clustering periods. The contour lines show the 95th (blue), 98th (green), 99th (red), and the 99.9th (magenta) percentiles of the local monthly IVT values.

along the eastern flank of the PV streamer/cutoff (Fig. 5a). The trough is reflected in the upper-level wind field, as can be seen in the Hovmöller diagrams of the meridional wind at 325 K calculated along the dynamical tropopause (i.e., the 2-PVU contour, $1\,\mathrm{PVU} = 10^{-6}\,\mathrm{K\,kg^{-1}\,m^2\,s^{-1}}$; Fig. 6a). A southerly upper-level flow is present over the eastern North Atlantic until 23 September, which is when the streamer evolved into a cutoff and when the signal is no longer traced by this Hovmöller diagnostic. On 2 October, a trough was

located over western Europe and again substantial moisture fluxes (>99.9%) were directed along the eastern flank of the trough toward the Alps (Fig. 5b). On 8 and 12 October, breaking waves and troughs were present over the easternmost Atlantic and western Europe (Figs. 5c,d).

Similar patterns are found for all other episodes; during each extreme precipitation event that occurred during the 1965, 1993, 2000, and 2002 clustering periods, a positive upper-level PV anomaly was present over western Europe (Fig. 5). The anomalies adopted the shape of a PV streamer, a broader PV trough, or a PV cutoff. They all reflect various stages of synoptic-scale Rossby wave breaking. This is in good agreement with previous findings that show that almost all heavy precipitation events in southern Switzerland are triggered by upper-level breaking waves and cutoffs located over western Europe (e.g., Massacand et al. 1998; Martius et al. 2006b). The upper-level PV anomalies are reflected in the upper-level flow as negative–positive meridional wind couplets (Fig. 6). The low-level flow associated with these upper-level PV structures transported significant amounts of moisture toward the Alps (Fig. 5); the moisture flux exceeded the local 95th percentile for every extreme precipitation events in the 1993, 2000, and 2002 clustering periods and for the first and last episode in 1965 (Fig. 5). When the moist air reached the Alps it was forced to rise, resulting in substantial amounts of precipitation (e.g., Doswell et al. 1998; Massacand et al. 1998). Indeed, the amplitude of the southerly moisture flux toward the Alps is the main characteristic that distinguishes wave breaking events over western Europe from wave breaking events that trigger heavy precipitation events (Martius et al. 2006b). The events ended with the dissipation or eastward translation of the upper-level anomalies. Each event was associated with its own PV structure aloft, confirming that the removal of high-frequency clustering from the extreme precipitation data successfully results in the identification of synoptically independent events.

In summary, every upper-tropospheric anomaly was associated with an upper-level breaking Rossby wave and a low-level southeasterly to southwesterly wind flow transporting significant amounts of moisture toward the south side of the Alps.

### e. *Upstream wave precursors*

To identify the possible mechanism(s) responsible for the subseasonal clustering, we analyze the mechanisms leading to Rossby wave breaking over western Europe and the upstream precursor Rossby waves to then identify the cause(s) for the repeated wave breaking and/or wave triggering in a short period of time. For Rossby wave breaking to occur, a linear Rossby wave must amplify strongly in the meridional direction to encounter critical lines (McIntyre and Palmer 1983). We will therefore look into the processes that led to the wave amplification and wave breaking and into linear precursor wave trains for every clustering period.

#### 1) THE 1993 EPISODE

All heavy precipitation events in fall 1993 were associated with a breaking synoptic-scale Rossby wave at upper levels (Fig. 5). The streamer/cutoff that formed on 23 September was preceded by a Rossby wave train extending from the eastern Pacific across North America and into the Atlantic (Fig. 6a). A strong cyclogenesis event over eastern North America on 21 September had resulted in the amplification of a ridge over the Atlantic through diabatic processes and subsequently in wave breaking and the formation of this PV streamer over western Europe (Massacand et al. 2001).

On 1 October, a transitioning tropical depression (TD10) interacted with an existing trough over North America (Figs. 7a,b). The following evidence suggests that this interaction played a role in the formation of the breaking wave on 2 October. TD10 can be seen in the IR satellite image on 1 October 1993 as it moved northward along the eastern flank of a preexisting trough located over eastern Canada (Figs. 7a–d). The former tropical system transported very large amounts of moisture northward (>99.9th local percentile; not shown) and the associated diabatic processes were very strong, as indicated by the cloud bands in Fig. 7a and the presence of WCB outflow air in the vicinity of TD10 at upper levels (Fig. 7a). The strong diabatic processes eroded the PV in the upper troposphere near the dynamical tropopause and in consequence very low PV was located south of the dynamical tropopause in the ridge and along the western flank of the trough over the western Atlantic (Figs. 7a,c). In addition, an area of strong divergent upper-level flow was present along the eastern flank of the trough over eastern Canada on 30 September and 1 October (Fig. 7b). This divergent flow formed primarily in response to strong diabatic processes associated with TD10.

The upper-level low PV strengthened the ridge over the Atlantic and the associated wind field assisted in the formation of the PV trough and later PV streamer over western Europe. The PV trough was associated with an extreme precipitation event in southern Switzerland on 2 October (Fig. 5b). The former tropical depression then underwent reintensification and propagated across the Atlantic. At upper levels the associated trough (called ET trough hereafter, for extratropical trough) moved slowly across the Atlantic. A strong blocking ridge

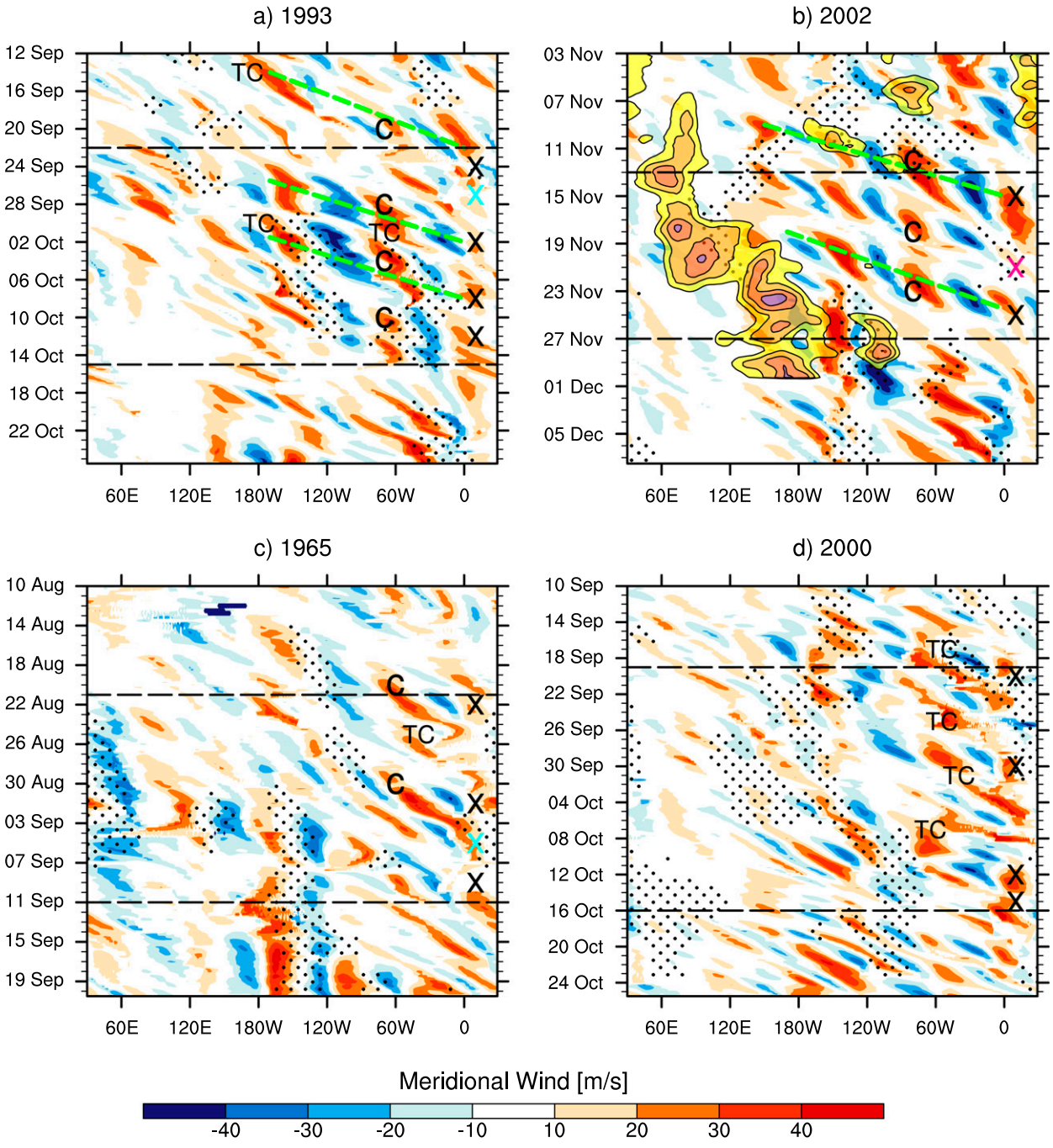


FIG. 6. Hovmöller plots of the meridional wind along the dynamical tropopause on the 325-K isentropic surface (shading, m $s^{-1}$) for (a) 0000 UTC 12 Sep–1800 UTC 24 Oct 1993, (b) 0000 UTC 3 Nov–1800 UTC 6 Dec 2002, (c) 0000 UTC 10 Aug–1800 UTC 19 Aug 1965, and (d) 0000 UTC 10 Sep–1800 UTC 24 Oct 2000. Positive (negative) values indicate poleward (equatorward) flow. Stippling indicates atmospheric blocking averaged between 40° and 70° latitude. Green dashed lines show wave trains. The yellow shading in (b) shows daily running average velocity potential anomalies at 250 hPa averaged over 0°–20°N for −4, −6, −8, and −10 $10^6$ $m^2$ $s^{-1}$. The label marks indicate the longitude of recurving cyclones (TC), low-level cyclones (C), and the time of extreme (>99th percentile) events (×). The very heavy (>98th percentile) and heavy (>95th percentile) precipitation events are marked in pink and blue, respectively.

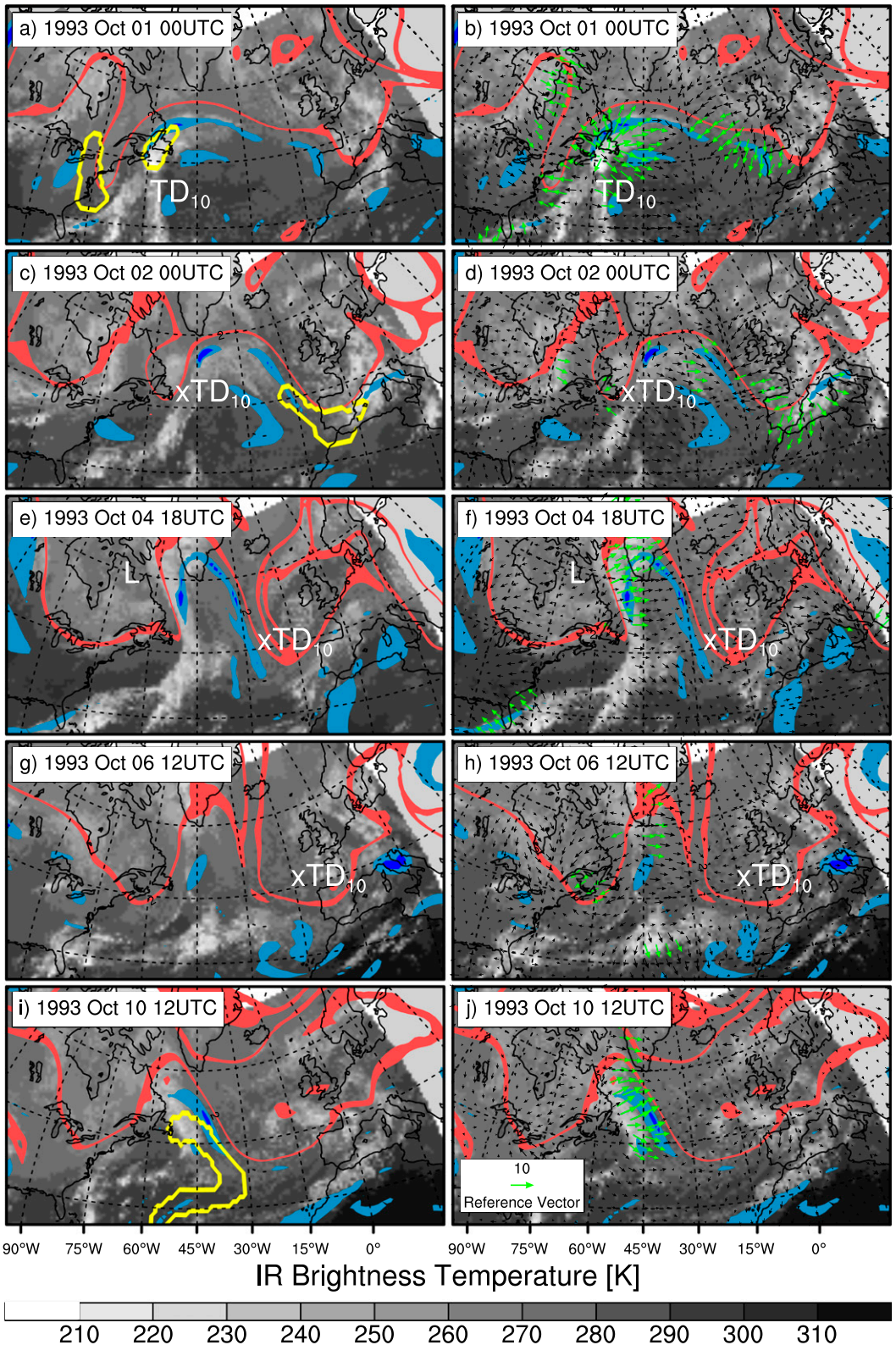


FIG. 7. Fall 1993 satellite imagery of IR brightness temperature and superimposed PV fields on the 325-K isentropic level (red = 2–3 PVU contour, blue ≤ 0.2 PVU, dark blue ≤ 0 PVU). The yellow contours show warm conveyor belt objects and the arrows [green ($\geq 10\ m\ s^{-1}$) and black ($<10\ m\ s^{-1}$)] show the vertically averaged (300–200 hPa) divergent wind field. The position of tropical depression TD10 and its extratropical continuation is labeled in white.

over the western Atlantic (Figs. 7e and 6a) contributed to the meridional elongation and southward extension of the broad ET trough over the eastern Atlantic (Figs. 7e,f). The ET trough then triggered the next heavy precipitation event from 6 to 8 October (Figs. 5c and 7g,h). Shortly thereafter, another ridge formed over the central Atlantic on 10 October in conjunction with cyclonic activity over North America, as evident from the presence of WCB air and upper-level divergent flow (Figs. 7i,j). This once again enhanced the equatorward extension of a mid-Atlantic cutoff over the eastern Atlantic (not shown). The cutoff evolved into a broad trough, which resulted in the last extreme precipitation event of the 1993 clustering period on 12 October (Fig. 5d).

#### 2) THE 2002 EPISODE

During the November 2002 clustering period, each extreme event was preceded by an upstream Rossby wave train with similar phase structure, triggered over the Pacific basin (Fig. 6b). The first Rossby wave train started over the western Pacific on 8 November. On 11 and 12 November 2002, a strong cyclogenesis event over the eastern coast of North America strengthened the ridge over the central Atlantic and thereby contributed to the southward extension of a preexisting trough over the eastern Atlantic (Fig. 8). This trough was then associated with an extreme precipitation event from 14 to 16 November 2002 (Fig. 5e). The next strong cyclogenesis event over the western Atlantic on 14 and 15 November 2002 further contributed to the strengthening of the ridge over the central Atlantic. The ridge over the Atlantic and a second strong ridge downstream of the trough over eastern Europe potentially contributed to the equatorward extension of the upper-level anomaly over the eastern Atlantic on 15 November (Fig. 5e). The next wave train formed over Asia and the eastern Pacific. Yet again, strong cyclogenesis occurred over Newfoundland a couple of days later on 24 November (Fig. 8c), followed by a ridge over the North Atlantic, which contributed to the equatorward extension of an upper-level anomaly over western Europe and resulted in the next extreme precipitation event on 25 November (Fig. 5f). The triggering of the wave trains will be discussed in section 3f(2).

#### 3) THE 1965 EPISODE

On 21 August 1965, an enhanced ridge over the North Atlantic supported the formation of a PV streamer over western Europe associated with the extreme precipitation event on 22 August (Figs. 5g and 9a,b). An anticyclone was located downstream over eastern Europe, which became a blocking anticyclone on 23 August (Fig. 6c, stippling), which prevented the eastward propagation of the breaking wave and potentially assisted the southward extension of the PV streamer through the associated deformation field (Fig. 9b). A trough located between two strong anticyclones can be elongated in the meridional direction by the deformation field exerted by the two anticyclones (e.g., Knippertz and Martin 2007; Moore et al. 2008). On 29 and 30 August, a cyclogenesis event over Newfoundland was followed by another ridge over the North Atlantic (Figs. 9c–f). This ridge, in conjunction with the blocking anticyclone located downstream over eastern Europe (Fig. 6c, stippling; see also Figs. 9c,e), contributed to the meridional elongation of the PV streamer/cutoff over western Europe associated with the next precipitation event on 1 September (Fig. 5h). On 7 September, a strong cyclogenesis event over the Hudson Bay (Fig. 9h) was followed by another high-latitude ridge over Greenland and resulted in a wave breaking event over the eastern Atlantic. The blocking anticyclone over eastern Europe prevented the eastward propagation of this PV trough (Fig. 9g). The next cyclogenesis event occurred over Newfoundland on 9 September and enhanced a next ridge over the Atlantic (Fig. 9j), which contributed to a further meridional elongation of the PV trough over western Europe (Figs. 9i,j) that resulted in the extreme event on 10 September (Fig. 5i).

#### 4) THE 2000 EPISODE

The extratropical waveguide can be disturbed when a tropical cyclone moves poleward and interacts with the waveguide (e.g., Riemer and Jones 2010; Archambault et al. 2013). In case of an optimal phasing of a tropical cyclone's path with the extratropical Rossby wave, diabatic processes and the divergent outflow associated with transitioning tropical cyclones can enhance downstream ridging over the Atlantic. As a result, meridionally elongated troughs form over western Europe (e.g., Grams et al. 2011; Pantillon 2012). During the 1993 clustering episode, the interaction of a transitioning tropical cyclone (TD10) with an extratropical Rossby wave was important for two of the four extreme precipitation events, as described above (see also Fig. 7).

During the 2000 clustering period, a series of recurving tropical cyclones in the Atlantic basin played an important role in the formation of the PV streamers that triggered the extreme precipitation events. The first event on 20 September (Figs. 5j) occurred downstream of the extratropical transition of Hurricane Florence. The extratropical transition contributed to the formation of a highly amplified blocking ridge over the central Atlantic (Figs. 10a,b) and the downstream development of the PV streamer associated with a heavy precipitation event (Figs. 10c,d). Former Hurricane Helene became embedded in the PV streamer associated with

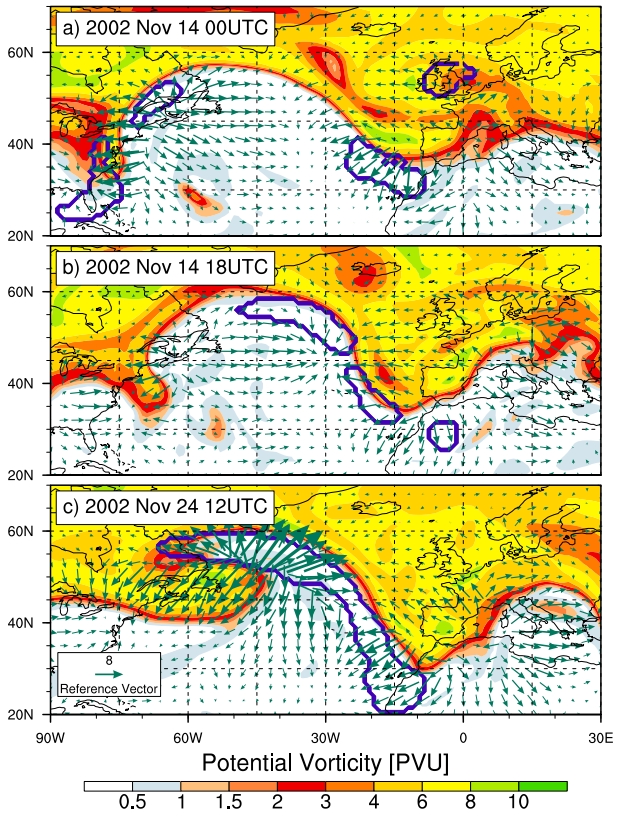


FIG. 8. PV field on the 325-K isentropic level (color shading), vertically averaged (300–200 hPa) divergent wind field (green arrows), and warm conveyor belt objects (purple) for the November 2002 events.

the second heavy precipitation event on 30 September (Figs. 10e,f and 5k); a block located downstream over eastern Europe (Figs. 6d and 10f) potentially supported the trough amplification. On 10 October, the remnants of Tropical Storm Leslie merged with a preexisting low pressure system over the eastern Atlantic. The upper-level trough associated with this system extended southward between a strong ridge located upstream over the Atlantic and a block downstream over eastern Europe and triggered the next extreme precipitation event on 12 October (Figs. 10g,h and 5l). In September and October 2000, six recurving tropical cyclones occurred in the North Atlantic (NA) basin (two in September and four in October).

Such a high number of tropical cyclones crossing the 40° latitude in the NA basin had previously only been observed in 1961 (not shown). In fall 2000 and in conjunction with a blocking ridge over eastern Europe, the frequency of recurving tropical cyclones played a central role for the successive occurrence of extreme precipitation events in southern Switzerland.

In summary, in two clustering episodes (1965 and 2000), blocking anticyclones downstream of Switzerland were of central importance. The two other episodes (1993 and 2002) reveal coherent upstream precursor wave signals extending into the Pacific for each extreme precipitation event. The clustering episodes of 1993 and 2000 are furthermore characterized by the occurrence of one or several recurving tropical cyclones. In most cases, upstream diabatic processes over North America and the western Atlantic were important for the amplification of the flow and the subsequent RWB over the eastern Atlantic and western Europe.

### *f. Factors contributing to the subseasonal clustering*

With the information on the atmospheric precursors, it is now possible to investigate the causes of subseasonal clustering of extreme precipitation events (i.e., which factors led to the repeated occurrence of extreme precipitation on time periods of 10–20 days). To this end, we focus on processes with time scales comparable to the length of a clustering period. Here, blocking, tropical forcing, and oceanic forcing are discussed.

#### 1) ROLE OF SST ANOMALIES

First, the oceanic surface conditions are discussed. The occurrence of subseasonal clustering of extreme precipitation events in southern Switzerland requires sufficient moisture supply. The primary moisture sources for extreme precipitation events on the Alpine south side are the eastern Atlantic and the Mediterranean (Duffourg and Ducrocq 2011; Turato et al. 2004; Winschall et al. 2012, 2014); it is therefore interesting to investigate sea surface temperature (SST) and precipitable water anomalies that prevailed during the clustering periods in order to identify anomalously high SSTs and amounts of moisture.

In three out of four clustering episodes, SST anomalies in the eastern Atlantic and the Mediterranean were either extremely weak or slightly but not significantly negative (Figs. 11a–c). This is consistent with the presence of the upper-level troughs and attendant cold air advection over western Europe (Fig. 12). This already suggests that SST anomalies were not relevant for moisture supply during the clustering of extreme precipitation events in southern Switzerland. During the 2002 clustering episode, positive SST anomalies (Fig. 11d) in tandem with slightly significant [>1.5 standard deviation (STD)] positive lower-tropospheric temperature anomalies in the western Atlantic (Fig. 12d) potentially contributed to enhanced baroclinicity in the western Atlantic and thereby to the intense cyclogenesis events over eastern North America [see also discussion in section 3e(4)].

Precipitable water anomalies show no systematic patterns over Europe; they are positive in 2002 (>2 STD) and 2000 (>1 STD) but extremely weak in 1965 and 1993

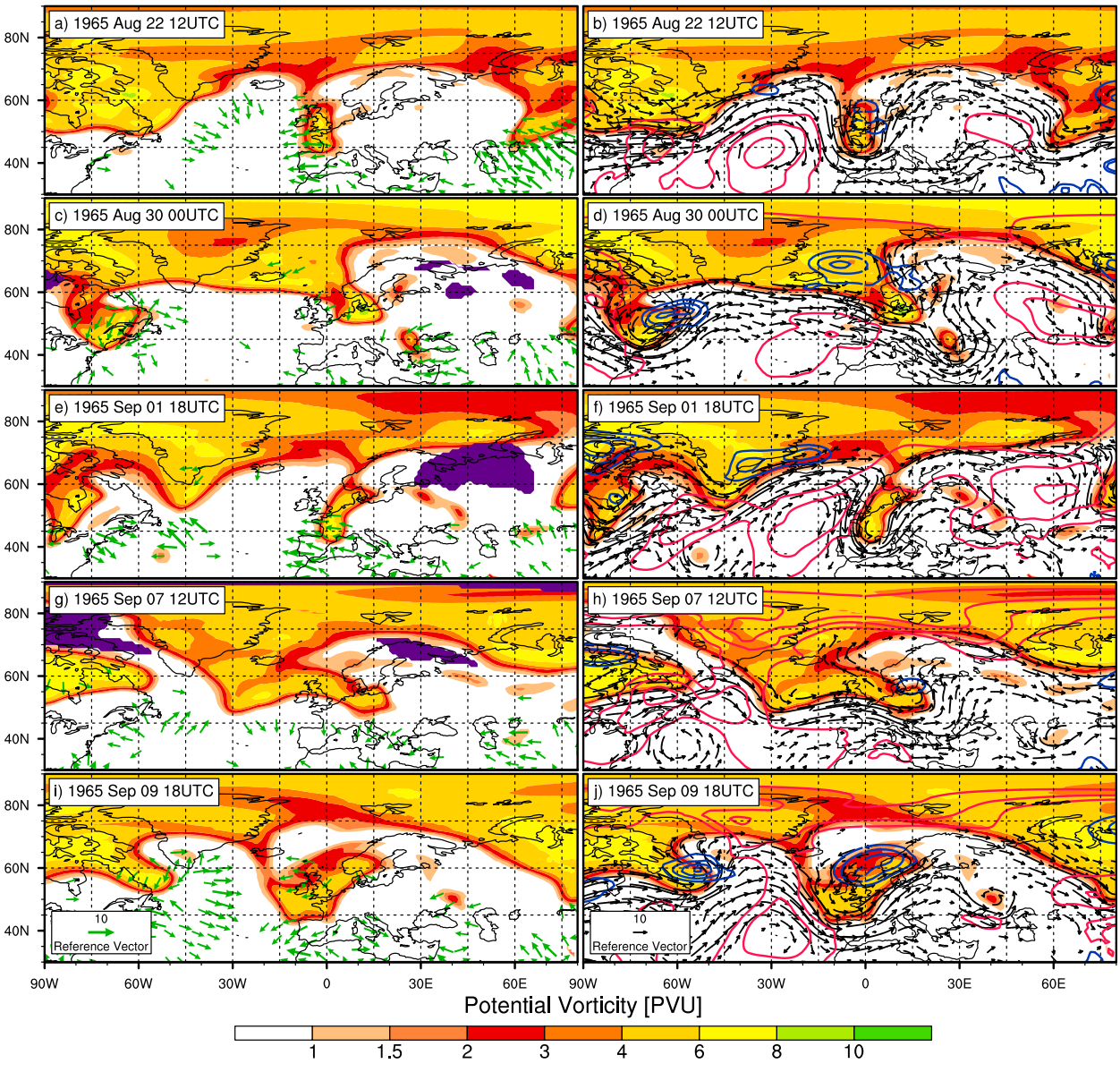


FIG. 9. (a),(c),(e),(g),(i) PV field on the 320-K isentropic level (color shading), vertically averaged (300–200 hPa) divergent wind field $\geq 5\ \mathrm{m\ s^{-1}}$ (green arrows), and blocking (purple shading) for the August–September 1965 events. (b),(d),(f),(h),(j) PV field (color shading) and wind vectors $\geq 5\ \mathrm{m\ s^{-1}}$ (black arrows) on the 320-K isentropic level and SLP [pink (≥1020 hPa) and blue (≤1000hPa) contours].

(Fig. 11). The extreme moisture fluxes on the Alpine south side are hence determined not only by the amount of precipitable water in the area but also by the magnitude of the wind responsible for the moisture advection.

### 2) ROLE OF THE TROPICS

We will next discuss the role of tropical forcing. The clustering periods of 1993 and 2002 were both characterized by a series of wave trains that formed in the Eastern Hemisphere, crossed the Pacific and the Atlantic, and ended with a wave breaking event over western Europe (Figs. 6a,b). These wave trains exhibited a very coherent phase structure during the clustering period (Fig. 6). Each of these wave trains triggered a heavy or extreme precipitation event. Before and after the clustering period, the phase coherence of the wave trains was lost. The processes responsible for the repeated wave train initiation are therefore of interest.

The upper-level divergent flow associated with strong tropical convection (e.g., during an active MJO event) can trigger and influence Rossby wave trains in the extratropics (Hoskins and Karoly 1981). During the 2002 clustering

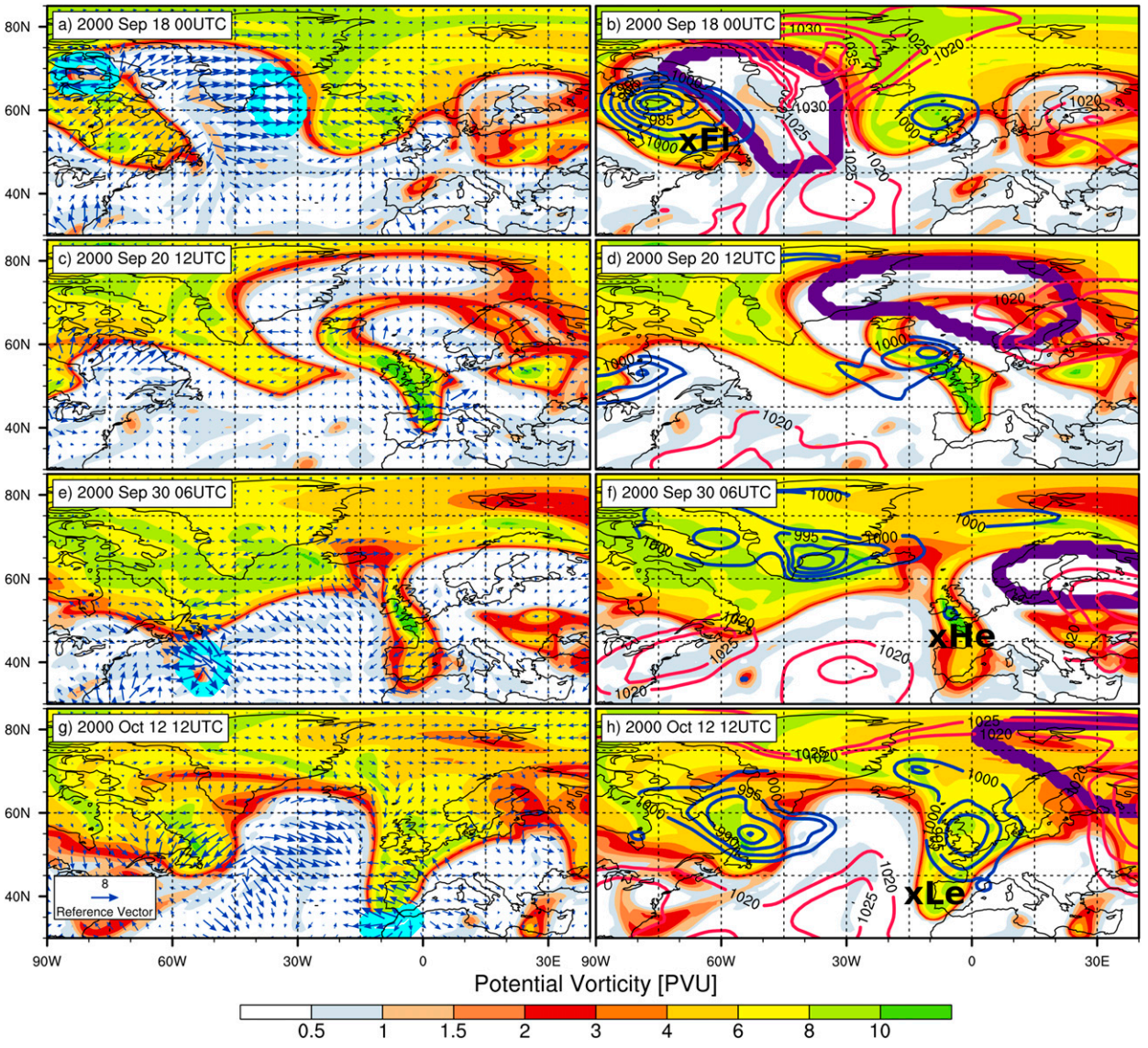


FIG. 10. (a),(c),(e),(g) PV field on the 325-K isentropic level (color shading), vertically averaged (300–200 hPa) divergent wind field (blue arrows), and warm conveyor belt objects (blue contours) for the September–October 2000 events. (b),(d),(f),(h) PV field (color shading), SLP [pink (≥1020 hPa) and blue (≤1000 hPa) contours], and blocking (purple contours). The extratropical continuation of Tropical Cyclones Florence (×Fl), Helen (×He), and Leslie (×Le) are labeled in black.

period, the magnitude of the MJO index (above 2) and its phase (2 and 3) indicate a very active MJO that prevailed in the Indian Ocean throughout the entire clustering period. A phase 2 MJO is characterized by anomalously low OLR values in the Indian Ocean between 60° and 90°E (Cassou 2008), an indication for deep tropical convection and upper-level divergence in this area.

This MJO event played a role in the triggering of the Rossby wave trains that preceded the heavy and extreme precipitation events during this clustering episode. Upper-tropospheric velocity potential anomalies (Fig. 6b) indicate regions of upper-level divergence between 60° and 120°E. The link between the upper-level divergent flow in the tropics and the Rossby wave trains forming in the extratropics is illustrated in more detail in Fig. 13. Figures 13a–c show OLR, streamfunction anomalies, and the divergent wind field and PV at tropopause levels on 7, 11, and 18 November 2002. These are roughly the dates when the wave trains that resulted in RWB and extreme precipitation in southern Switzerland were triggered over Asia and the eastern Pacific (Fig. 6b). The MJO-related strongly divergent upper-level flow over the eastern Indian Ocean contributed to the amplification of a first wave train that formed around 7 November, reached western

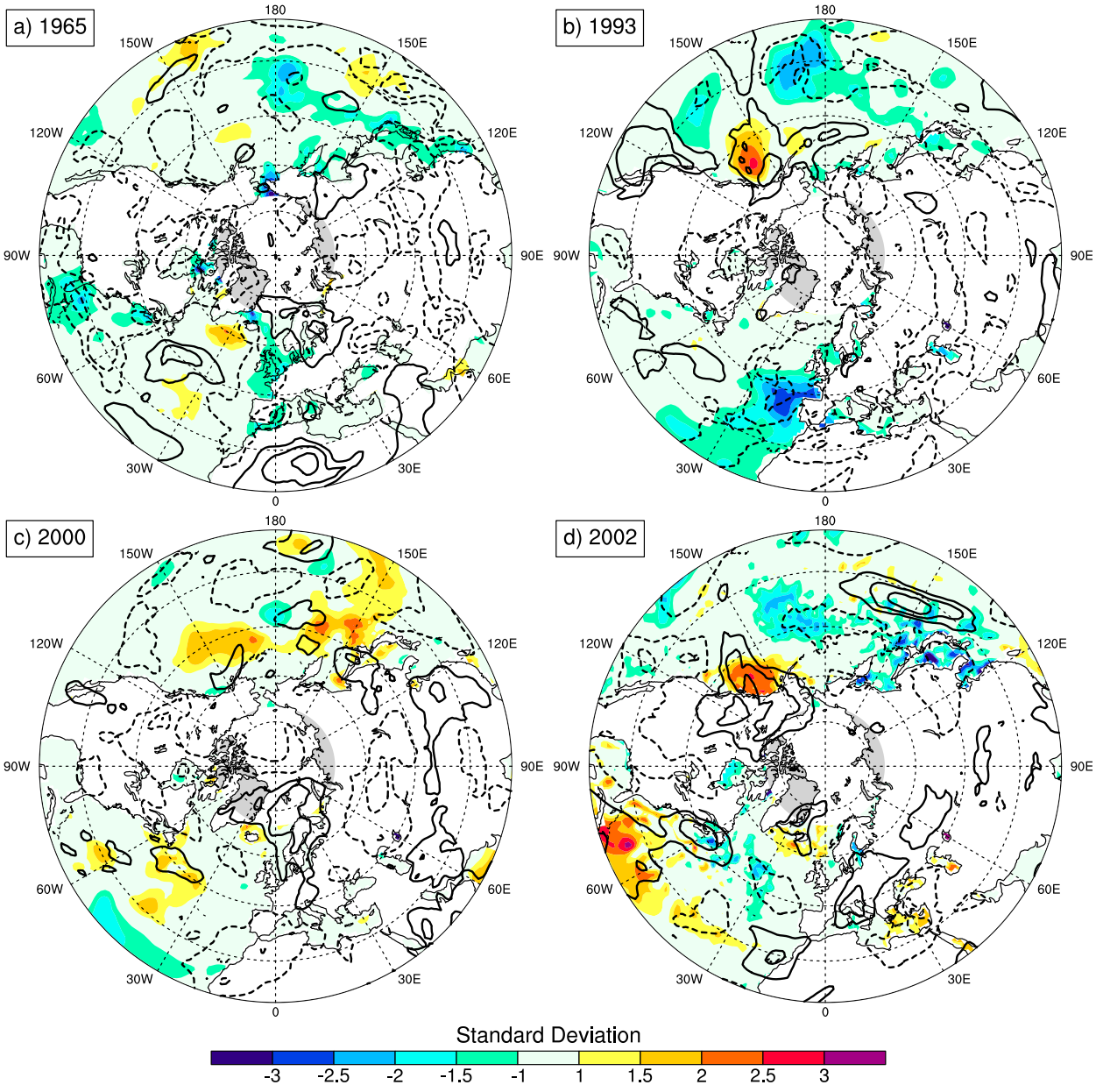


FIG. 11. Composites of daily standardized SST anomalies for all days between (a) 21 Aug and 11 Sep 1965, (b) 22 Sep and 15 Oct 1993, (c) 19 Sep and 16 Oct 2000, and (d) 13 and 27 Nov 2002. The black solid (dashed) contour lines show positive (negative) standardized precipitable water anomalies. Contour interval is one standard deviation.

Europe around 12 November, and triggered an extreme precipitation event on 15 November. However, extratropical disturbances were involved in the triggering of this wave train as well (Fig. 13a). The wave train was initiated by the two anticyclonic flow anomalies centered at 45°N, 90°E and at 25°N, 110°E (Fig. 13a). The MJO-related signal is the anticyclonic flow anomaly (i.e., the Rossby wave response to tropical heating; Gill 1980; Barlow et al. 2007), located at 100°–120°E. The second wave train was triggered by the strong anticyclonic flow anomaly centered at 27°N, 105°E on 11 November 2002 (Fig. 13b), again directly related to strongly divergent flow at 80°E. The third wave train was triggered by the strong anticyclonic flow anomaly over the Indian subcontinent on 17 and 18 November 2002 (Fig. 13c), when strong convection was present between 70° and 110°E and associated divergent upper-level winds at 90° and 120°E.

During the other clustering episodes the role of the MJO is less evident. In September 1993 the MJO was very weak, in late September and early October 2000 the MJO

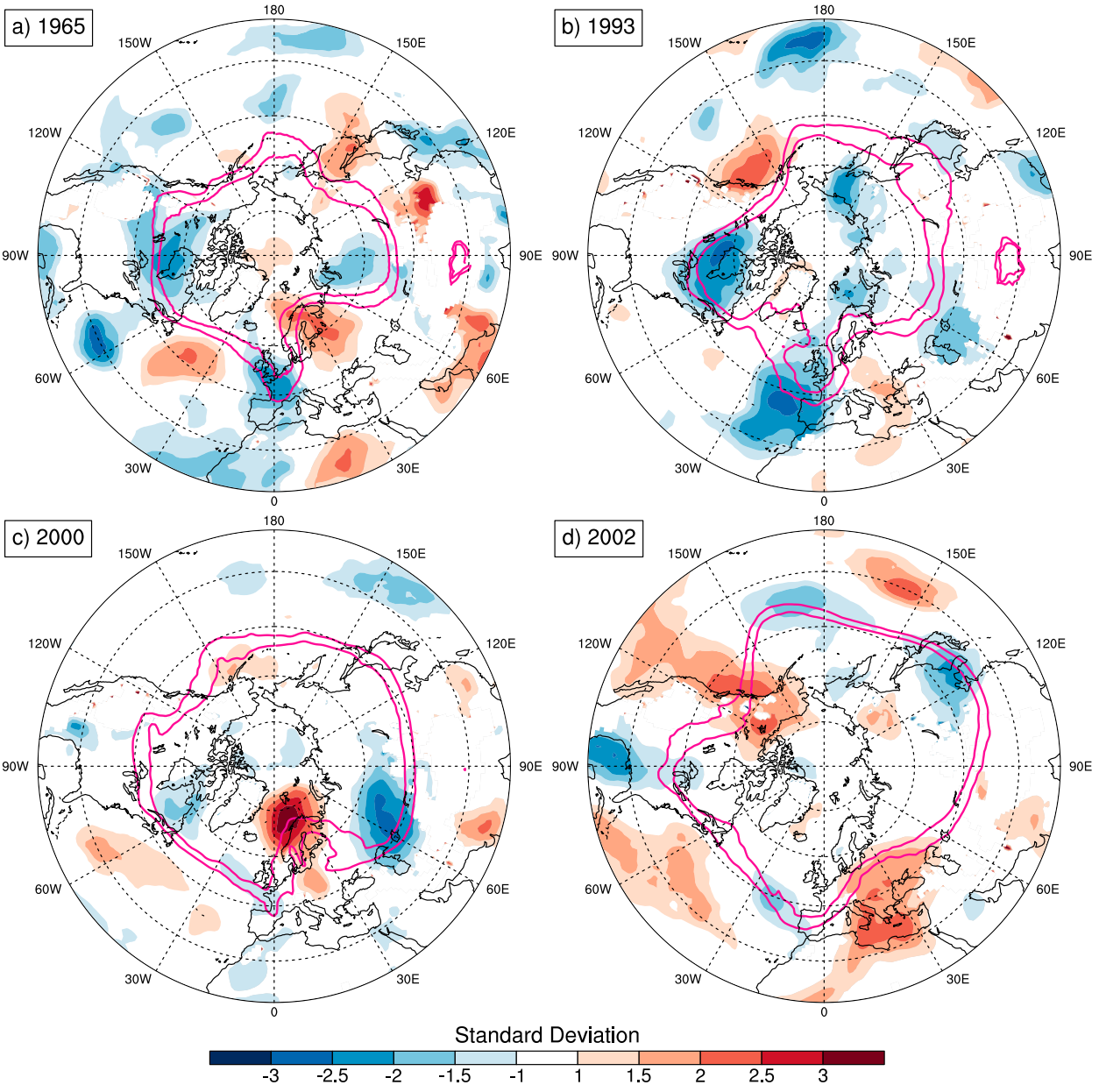


FIG. 12. Composites of daily standardized temperature anomalies at 850 hPa for all days between (a) 21 Aug and 11 Sep 1965, (b) 22 Sep and 15 Oct 1993, (c) 19 Sep and 16 Oct 2000, and (d) 13 and 27 Nov 2002. The 2- and 3-PVU contour lines on the 325-K isentropic level averaged over the same time periods are shown in pink.

was active in the Indian Ocean basin, and for August 1965 we do not have information about the state of the MJO because this time period falls into the presatellite area.

A second relevant tropical influence on extratropical wave trains is recurving tropical cyclones. Several recurving tropical cyclones occurred prior to and during the 1993 and the 2000 clustering episodes (Figs. 6, 7, and 10) and their role in amplifying the flow upstream of western Europe is discussed in detail in section 3. A tropical and subtropical flow setting that is conducive to the repeated formation and recurvature of tropical cyclones can hence also favor the clustering of precipitation extremes over southern Switzerland.

### 3) ROLE OF THE BLOCKING ANTICYCLONES

Blocking anticyclones were present both upstream and downstream of Switzerland during several clustering episodes. We first discuss the role of blocking located upstream of Europe during the 1993 clustering period. In 1993, a strong blocking anticyclone was present over the

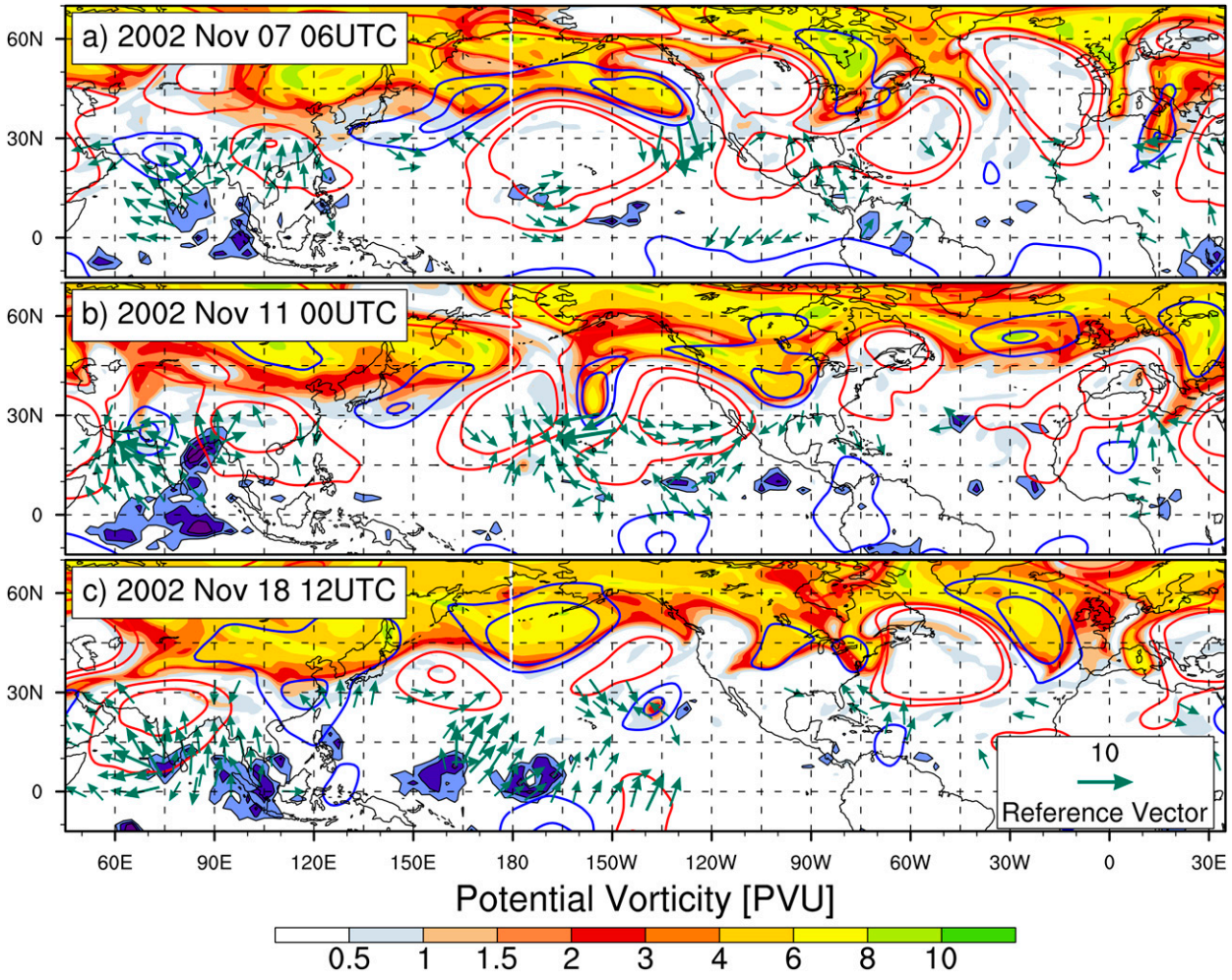


FIG. 13. PV field on the 325-K isentropic level (color shading), streamfunction anomalies to the 1979–2013 base period monthly means at 250 hPa ($1 \times 10^7$ and $2 \times 10^7\ s^{-1}$ in solid red contours, $-1 \times 10^7$ and $-2 \times 10^7\ s^{-1}$ in blue contours), vertically averaged (300–200 hPa) divergent wind field $\geq 5\ m\ s^{-1}$ south of 40°N (green arrows), and OLR south of 30°N (180, 150, and 120 $W\ m^{-2}$ in bright to dark blue shading respectively).

Gulf of Alaska from 29 September onward (Fig. 6a). The role of this blocking anticyclone was potentially threefold. First, it ensured a phase locking of the flow downstream. Second, cold air advection along the eastern flank of the block resulted in a very significant cold air anomaly over North America (Fig. 12). Third, there was recurrent trough formation and (anticyclonic) wave breaking along the eastern flank of the block. The last two points were potentially crucial for the intense cyclogenesis events over eastern North America. Lackmann et al. (1996) found that the successive formation of troughs over North America is more likely to occur in the presence of a blocking ridge over western North America. Furthermore, the upper-level troughs provide quasigeostrophic support for the triggering of cyclogenesis over the eastern North American continent; the cold air advected in a northwesterly flow tends to further increase the baroclinicity along the eastern seaboard (Lackmann et al. 1996). Simultaneous blocking over the Atlantic further assisted the phase locking of the waves and the wave breaking downstream over western Europe, as observed during the 1993 episode (see Fig. 6a).

The role of blocking located downstream of Switzerland is best illustrated with the 1965 and 2000 periods. During the clustering period of August 1965, a persistent blocking anticyclone was located downstream over eastern Europe (Figs. 6c, 9, and 14a). Similarly, there was also a block present over eastern Europe during all three extreme precipitation events in October 2000 (Figs. 6d, 10, and 14b). These blocks ensured the stationarity of the flow and repeated wave breaking over western Europe (Figs. 6, 9, and 10). Between the breaking wave and the block downstream, strong synoptic-scale ascent potentially assisted the formation

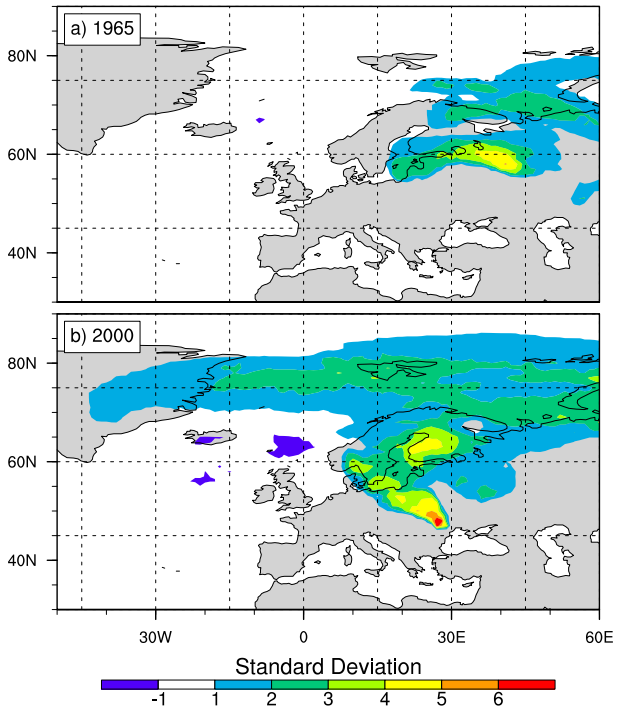


FIG. 14. Standardized blocking frequency in standard deviations for August 1965 and September and October 2000.

of extreme precipitation. The more or less continuous presence of blocking anticyclones over eastern Europe in summer is highly unusual. Figure 14 shows the standardized blocking frequency anomaly during the months of August 1965 and September/October 2000. The blocking frequency anomalies reach up to four standard deviations over parts of eastern Europe, Scandinavia, and western Russia, indicating how unusual the large-scale flow situation over Europe was.

## 4. Conclusions

Temporal clustering of regional-scale extreme precipitation events in southern Switzerland on subseasonal time scales has significant hydrological and societal consequences. We have studied the statistical properties of clustering and the synoptic large-scale flow conditions that led to the extreme events. We have analyzed and quantified subseasonal clustering of precipitation extremes using a variant of Ripley's $K$ function, which is a useful and simple to apply tool to compare the clustering properties of the data on subseasonal time scales with a homogeneous Poisson model. Extreme regional-scale precipitation events in southern Switzerland are typically triggered by synoptic systems with a lifetime of more than one day, resulting in an autocorrelation of the extreme precipitation days that we call high-frequency clustering. This high-frequency clustering affects the clustering on longer subseasonal time scales and was therefore removed from the time series before investigating clustering on subseasonal time scales. After declustering of the extreme precipitation time series, statistically significant clustering was found in fall on time scales from 10 to 20 days, and for the most extreme events for time scales longer than 20 days. The remaining seasons exhibited extreme precipitation events consistent with a Poisson point process and hence no clustering. Then, four episodes with multiple extreme precipitation events occurring within a subseasonal time span were analyzed in detail. From these few case studies we learned the following:

- During all clustered heavy and extreme precipitation events, an independent synoptic-scale Rossby wave breaking event in the form of an elongated trough or a cutoff was present over western Europe. This flow configuration ensured extreme poleward moistures fluxes on the forward flank of the upper-level anomaly toward the Alpine ridge, which resulted in extreme precipitation.
- The Rossby wave breaking events over western Europe themselves were preceded in many cases by a strong ridge upstream over the central Atlantic and by strong cyclogenesis or extratropical transition events farther upstream over the western Atlantic or North America. The intense diabatic processes associated with these cyclonic systems strengthened the ridges over the Atlantic and the strong ridges in return contributed to the southward extensions of the breaking waves over western Europe. This is in line with previous studies that have assessed the mechanisms contributing to downstream upper-level wave amplification and subsequent wave breaking over western Europe and the findings of Pfahl et al. (2015). They indicate also the crucial role of diabatic processes associated with strong cyclogenesis (e.g., Massacand et al. 2001; Madonna et al. 2014b) or the extratropical transition over the western Atlantic (e.g., Archambault et al. 2013; Grams et al. 2011; Pantillon 2012).
- Atmospheric blocking contributed to clustering of extreme precipitation events. During two episodes (1965 and 2000), a blocking anticyclone was present over eastern Europe downstream of the breaking wave. The blocking anticyclone assisted the wave breaking over western Europe and played a major role in determining the recurrent occurrence of wave breaking at this specific location. During the fall 1993 episode, a blocking anticyclone over the eastern Pacific ensured the phase locking of the upper-level Rossby wave pattern for a 10-day time period. The blocking further assisted

the advection of cold air and the formation of a trough directly downstream over eastern North America as well as a second ridge–trough couplet downstream over the Atlantic.

- Tropical forcing was identified as a second contributor to clustering of extreme precipitation events. In fall 2000, the extratropical transition of a series of hurricanes played a relevant role in the amplification of the extratropical flow. During this episode, most of the extreme events occurred right after the extratropical transitions of tropical cyclones. During the 2002 episode, the upper-level Rossby wave pattern was phase-locked for approximately 15 days and precursor Rossby waves to the extreme precipitation events started in the Eastern Hemisphere. A very active MJO in the Indian Ocean contributed to the triggering of these waves.

In summary, the dynamical processes responsible for the recurrent formation of extreme precipitation events differ between the four investigated episodes. There is no single simple mechanism responsible for the clustering; instead, the clustering emanates from a complex interaction of a number of factors that are case specific. Nevertheless, several important mechanisms have been identified that can result in subseasonal clustering, either individually or in combination. These are processes active on longer, subseasonal time scales, namely 1) blocking anticyclones in the extratropics and 2) tropical forcing in the form of an active MJO or the recurrent recurvature of tropical cyclones. They arise from atmospheric internal variability only; no coherent forcing/effect of the ocean was found.

The central interest of this work was to perform a thorough analysis of the most extreme clustering periods, with a focus on the dynamical mechanisms and processes leading to the clustering; the predictability of clustering periods was not analyzed. An extension of the work presented here would be to systematically compare the dynamics resulting in isolated heavy precipitation events with the dynamics associated with clustered events. This would require a larger sample that would include also events with moderate impacts but would provide more information, such as about the predictability of subseasonally recurring extremes.

*Acknowledgments.* The authors thank Ron McTaggart-Cowan and two anonymous reviewers for their helpful feedback that greatly improved the quality of this manuscript. We wish to thank MeteoSwiss for providing access to the gridded observational precipitation data as well as the ERA-40 and ERA-Interim datasets. Thanks also go to the Swiss Federal Office for the Environment for providing the daily Lago Maggiore water level data and to Erica Madonna for the WCB objects. Paraskevi Giannakaki is funded by the Swiss Science Foundation Grant Number 200021_137543.

## REFERENCES

Archambault, H. M., L. F. Bosart, D. Keyser, and J. M. Cordeira, 2013: A climatological analysis of the extratropical flow response to recurving western North Pacific tropical cyclones. *Mon. Wea. Rev.*, **141**, 2325–2346, doi:10.1175/MWR-D-12-00257.1.

Badoux, A., and D. Rickenmann, 2008: Berechnungen zum Geschiebetransport während der Hochwasser 1993 und 2000 im Wallis. *Wasser Energ. Luft*, **100** (3), 217–226.

BAFU, 1994: Die Hochwasser 1993 im Wallis und Tessin—Messdaten und ausgesuchte Auswertungen. Bundesamt für Umwelt, 80 pp.

Barlow, M., A. Hoell, and F. Colby, 2007: Examining the wintertime response to tropical convection over the Indian Ocean by modifying convective heating in a full atmospheric model. *Geophys. Res. Lett.*, **34**, L19702, doi:10.1029/2007GL030043.

Cassou, C., 2008: Intraseasonal interaction between the Madden–Julian Oscillation and the North Atlantic Oscillation. *Nature*, **455**, 523–527, doi:10.1038/nature07286.

Coles, S., 2001: *An Introduction to Statistical Modeling of Extreme Values.* Springer, 208 pp.

Dee, D., and Coauthors, 2011: The ERA-Interim reanalysis: Configuration and performance of the data assimilation system. *Quart. J. Roy. Meteor. Soc.*, **137**, 553–597, doi:10.1002/qj.828.

Dixon, P. M., 2002: Ripley's K-function. *Encyclopedia of Environmetrics*, Vol. 3, A. H. El-Shaarawi and W. W. Piegorsch, Eds., John Wiley & Sons, 1796–1803.

Doswell, C. A., III, C. Ramis, R. Romero, and S. Alonso, 1998: A diagnostic study of three heavy precipitation episodes in the western Mediterranean region. *Wea. Forecasting*, **13**, 102–124, doi:10.1175/1520-0434(1998)013<0102:ADSOTH>2.0.CO;2.

Duffourg, F., and V. Ducrocq, 2011: Origin of the moisture feeding the heavy precipitating systems over southeastern France. *Nat. Hazards Earth Syst. Sci.*, **11**, 1163–1178, doi:10.5194/nhess-11-1163-2011.

Ferro, C. A., and J. Segers, 2003: Inference for clusters of extreme values. *J. Roy. Stat. Soc.*, **65B**, 545–556, doi:10.1111/1467-9868.00401.

Fischer, A., A. Weigel, C. Buser, R. Knutti, H. Künsch, M. Liniger, C. Schär, and C. Appenzeller, 2012: Climate change projections for Switzerland based on a Bayesian multi-model approach. *Int. J. Climatol.*, **32**, 2348–2371, doi:10.1002/joc.3396.

Frei, C., and C. Schär, 1998: A precipitation climatology of the Alps from high-resolution rain-gauge observations. *Int. J. Climatol.*, **18**, 873–900, doi:10.1002/(SICI)1097-0088(19980630)18:8<873::AID-JOC255>3.0.CO;2-9.

——, H. C. Davies, J. Gurtz, and C. Schär, 2000: Climate dynamics and extreme precipitation and flood events in Central Europe. *Integr. Assess.*, **1**, 281–300, doi:10.1023/A:1018983226334.

Fukutome, S., M. Liniger, and M. Süveges, 2015: Automatic threshold and run parameter selection: A climatology for extreme hourly precipitation in Switzerland. *Theor. Appl. Climatol.*, **120**, 403–416, doi:10.1007/s00704-014-1180-5.

Galarneau, T., Jr., T. Hamill, R. Dole, and J. Perlwitz, 2012: A multiscale analysis of the extreme weather events over western

Russia and Northern Pakistan during July 2010. *Mon. Wea. Rev.*, **140**, 1639–1664, doi:10.1175/MWR-D-11-00191.1.

Gill, A., 1980: Some simple solutions for heat-induced tropical circulation. *Quart. J. Roy. Meteor. Soc.*, **106**, 447–462, doi:10.1002/qj.49710644905.

Grams, C. M., and Coauthors, 2011: The key role of diabatic processes in modifying the upper-tropospheric wave guide: A North Atlantic case-study. *Quart. J. Roy. Meteor. Soc.*, **137**, 2174–2193, doi:10.1002/qj.891.

——, H. Binder, S. Pfahl, N. Piaget, and H. Wernli, 2014: Atmospheric processes triggering the Central European floods in June 2013. *Nat. Hazards Earth Syst. Sci.*, **14**, 1691–1702, doi:10.5194/nhess-14-1691-2014.

Grazzini, F., 2007: Predictability of a large-scale flow conducive to extreme precipitation over the Western Alps. *Meteor. Atmos. Phys.*, **95**, 123–138, doi:10.1007/s00703-006-0205-8.

Haase, P., 1995: Spatial pattern analysis in ecology based on Ripley's K-function: Introduction and methods of edge correction. *J. Veg. Sci.*, **6**, 575–582, doi:10.2307/3236356.

Hilker, N., A. Badoux, and C. Hegg, 2009: The Swiss flood and landslide damage database 1972–2007. *Nat. Hazards Earth Syst. Sci.*, **9**, 913–925, doi:10.5194/nhess-9-913-2009.

Hoinka, K. P., C. Schwierz, and O. Martius, 2006: Synoptic-scale weather patterns during Alpine heavy rain events. *Quart. J. Roy. Meteor. Soc.*, **132**, 2853–2860, doi:10.1256/qj.05.239.

Hoskins, B. J., and D. J. Karoly, 1981: The steady linear response of a spherical atmosphere to thermal and orographic forcing. *J. Atmos. Sci.*, **38**, 1179–1196, doi:10.1175/1520-0469(1981)038<1179:TSLROA>2.0.CO;2.

Huntingford, C., and Coauthors, 2014: Potential influences on the United Kingdom's floods of winter 2013/14. *Nat. Climate Change*, **4**, 769–777, doi:10.1038/nclimate2314.

Knapp, K. R., 2008: Scientific data stewardship of International Satellite Cloud Climatology Project B1 global geostationary observations. *J. Appl. Remote Sens.*, **2**, 023548, doi:10.1117/1.3043461.

——, M. C. Kruk, D. H. Levinson, H. J. Diamond, and C. J. Neumann, 2010: The International Best Track Archive for Climate Stewardship (IBTrACS): Unifying tropical cyclone data. *Bull. Amer. Meteor. Soc.*, **91**, 363–376, doi:10.1175/2009BAMS2755.1.

Knippertz, P., and J. E. Martin, 2007: The role of dynamic and diabatic processes in the generation of cut-off lows over northwest Africa. *Meteor. Atmos. Phys.*, **96**, 3–19, doi:10.1007/s00703-006-0217-4.

Lackmann, G. M., L. F. Bosart, and D. Keyser, 1996: Planetary- and synoptic-scale characteristics of explosive wintertime cyclogenesis over the western North Atlantic Ocean. *Mon. Wea. Rev.*, **124**, 2672–2702, doi:10.1175/1520-0493(1996)124<2672:PASSCO>2.0.CO;2.

Liebmann, B., and C. A. Smith, 1996: Description of a complete (interpolated) outgoing longwave radiation dataset. *Bull. Amer. Meteor. Soc.*, **77**, 1275–1277.

Madonna, E., S. Limbach, C. Aebi, H. Joos, H. Wernli, and O. Martius, 2014a: On the co-occurrence of warm conveyor belt outflows and PV streamers. *J. Atmos. Sci.*, **71**, 3668–3673, doi:10.1175/JAS-D-14-0119.1.

——, H. Wernli, H. Joos, and O. Martius, 2014b: Warm conveyor belts in the ERA-Interim dataset (1979–2010). Part I: Climatology and potential vorticity evolution. *J. Climate*, **27**, 3–26, doi:10.1175/JCLI-D-12-00720.1.

Mailier, P. J., D. B. Stephenson, C. A. Ferro, and K. I. Hodges, 2006: Serial clustering of extratropical cyclones. *Mon. Wea. Rev.*, **134**, 2224–2240, doi:10.1175/MWR3160.1.

Martius, O., C. Schwierz, and H. C. Davies, 2006a: A refined Hovmöller diagram. *Tellus*, **58A**, 221–226, doi:10.1111/j.1600-0870.2006.00172.x.

——, E. Zenklusen, C. Schwierz, and H. C. Davies, 2006b: Episodes of alpine heavy precipitation with an overlying elongated stratospheric intrusion: A climatology. *Int. J. Climatol.*, **26**, 1149–1164, doi:10.1002/joc.1295.

——, C. Schwierz, and H. Davies, 2008: Far-upstream precursors of heavy precipitation events on the Alpine south-side. *Quart. J. Roy. Meteor. Soc.*, **134**, 417–428, doi:10.1002/qj.229.

——, and Coauthors, 2013: The role of upper-level dynamics and surface processes for the Pakistan flood of July 2010. *Quart. J. Roy. Meteor. Soc.*, **139**, 1780–1797, doi:10.1002/qj.2082.

Massacand, A. C., H. Wernli, and H. C. Davies, 1998: Heavy precipitation on the Alpine southside: An upper-level precursor. *Geophys. Res. Lett.*, **25**, 1435–1438, doi:10.1029/98GL50869.

——, ——, and ——, 2001: Influence of upstream diabatic heating upon an Alpine event of heavy precipitation. *Mon. Wea. Rev.*, **129**, 2822–2828, doi:10.1175/1520-0493(2001)129<2822:IOUDHU>2.0.CO;2.

McIntyre, M. E., and T. Palmer, 1983: Breaking planetary waves in the stratosphere. *Nature*, **305**, 593–600, doi:10.1038/305593a0.

MeteoSwiss, 2013: Documentation of MeteoSwiss grid-data products—Daily precipitation (final analysis): RhiresD. MeteoSwiss, 4 pp.

Moore, R., O. Martius, and H. Davies, 2008: Downstream development and Kona low genesis. *Geophys. Res. Lett.*, **35**, L20814, doi:10.1029/2008GL035502.

Pantillon, F., 2012: Transition extra-tropicale d'ouragans en Atlantique Nord et impact sur la prévisibilité d'événements extrêmes en Méditerranée. Ph.D. thesis, Université Paul Sabatier-Toulouse III, 113 pp.

Pfahl, S., and H. Wernli, 2012: Quantifying the relevance of cyclones for precipitation extremes. *J. Climate*, **25**, 6770–6780, doi:10.1175/JCLI-D-11-00705.1.

——, C. Schwierz, M. Croci-Maspoli, C. Grams, and H. Wernli, 2015: Importance of latent heat release in ascending air streams for atmospheric blocking. *Nat. Geosci.*, **8**, 610–614, doi:10.1038/ngeo2487.

Pinto, J. G., N. Bellenbaum, M. K. Karremann, and P. M. Della-Marta, 2013: Serial clustering of extratropical cyclones over the North Atlantic and Europe under recent and future climate conditions. *J. Geophys. Res. Atmos.*, **118**, 12 476–12 485, doi:10.1002/2013JD020564.

——, I. Gómara, G. Masato, H. Dacre, T. Woollings, and R. Caballero, 2014: Large-scale dynamics associated with clustering of extra-tropical cyclones affecting Western Europe. *J. Geophys. Res. Atmos.*, **119**, 13 704–13 719, doi:10.1002/2014JD022305.

Riemer, M., and S. C. Jones, 2010: The downstream impact of tropical cyclones on a developing baroclinic wave in idealized scenarios of extratropical transition. *Quart. J. Roy. Meteor. Soc.*, **136**, 617–637, doi:10.1002/qj.605.

——, ——, and C. Davis, 2008: The impact of extratropical transition on the downstream flow: An idealized modeling study with a straight jet. *Quart. J. Roy. Meteor. Soc.*, **134**, 69–91, doi:10.1002/qj.189.

Ripley, B., 1981: *Spatial Statistics*. Wiley, 272 pp.

Schwierz, C., M. Croci-Maspoli, and H. Davies, 2004: Perspicacious indicators of atmospheric blocking. *Geophys. Res. Lett.*, **31**, L06125, doi:10.1029/2003GL019341.

Süveges, M., and A. C. Davison, 2010: Model misspecification in peaks over threshold analysis. *Ann. Appl. Stat.*, **4**, 203–221, doi:10.1214/09-AOAS292.

Turato, B., O. Reale, and F. Siccardi, 2004: Water vapor sources of the October 2000 Piedmont flood. *J. Hydrometeor.*, **5**, 693–712, doi:10.1175/1525-7541(2004)005<0693:WVSOTO>2.0.CO;2.

Uppala, S. M., and Coauthors, 2005: The ERA-40 Re-Analysis. *Quart. J. Roy. Meteor. Soc.*, **131**, 2961–3012, doi:10.1256/qj.04.176.

Villarini, G., J. A. Smith, M. L. Baeck, R. Vitolo, D. B. Stephenson, and W. F. Krajewski, 2011: On the frequency of heavy rainfall for the Midwest of the United States. *J. Hydrol.*, **400**, 103–120, doi:10.1016/j.jhydrol.2011.01.027.

Vitolo, R., D. B. Stephenson, I. M. Cook, and K. Mitchell-Wallace, 2009: Serial clustering of intense European storms. *Meteor. Z.*, **18**, 411–424, doi:10.1127/0941-2948/2009/0393.

Wheeler, M., and H. Hendon, 2004: An all-season real-time multivariate MJO index: Development of an index for monitoring and prediction. *Mon. Wea. Rev.*, **132**, 1917–1932, doi:10.1175/1520-0493(2004)132<1917:AARMMI>2.0.CO;2.

Winschall, A., S. Pfahl, H. Sodemann, and H. Wernli, 2012: Impact of North Atlantic evaporation hot spots on southern Alpine heavy precipitation events. *Quart. J. Roy. Meteor. Soc.*, **138**, 1245–1258, doi:10.1002/qj.987.

——, H. Sodemann, S. Pfahl, and H. Wernli, 2014: How important is intensified evaporation for Mediterranean precipitation extremes? *J. Geophys. Res. Atmos.*, **119**, 5240–5256, doi:10.1002/2013JD021175.